Micro-Scale In Vivo Human Electrophysiological Functional Connectivity During Simple Language Production and Parkinson's Disease

by

Kevin John O'Neill III

A Dissertation Presented in Partial Fulfillment
of the Requirements for the Degree
Doctor of Philosophy

Approved October 2021 by the
Graduate Supervisory Committee:

Bradley Greger, Chair
Marco Santello
Stephen Helms-Tillery
Antonia Papandreou-Suppapola
Jeffery Kleim

ARIZONA STATE UNIVERSITY

December 2021

ABSTRACT

Information processing in the brain is mediated by network interactions between anatomically distant (centimeters apart) regions of cortex and network action is fundamental to human behavior. Disruptive activity of these networks may allow a variety of diseases to develop. Degradation or loss of network function in the brain can affect many aspects of the human experience; motor disorder, language difficulties, memory loss, mood swings, and more.

The cortico-basal ganglia loop is a system of networks in the brain between the cortex, basal ganglia, the thalamus, and back to the cortex. It is not one singular circuit, but rather a series of parallel circuits that are relevant towards motor output, motor planning, and motivation and reward. Studying the relationship between basal ganglia neurons and cortical local field potentials may lead to insights about neurodegenerative diseases and how these diseases change the cortico-basal ganglia circuit.

Speech and language are uniquely human and require the coactivation of several brain regions. The various aspects of language are spread over the temporal lobe and parts of the occipital, parietal, and frontal lobe. However, the core network for speech production involves collaboration between phonologic retrieval (encoding ideas into syllabic representations) from Wernicke's area, and phonemic encoding (translating syllables into motor articulations) from Broca's area. Studying the coactivation of these brain regions during a repetitive speech production task may lead to a greater understanding of their electrophysiological functional connectivity.

The primary purpose of the work presented in this document is to validate the use of subdural microelectrodes in electrophysiological functional connectivity research as

these devices best match the spatial and temporal scales of brain activity. Neuron populations in the cortex are organized into functional units called cortical columns. These cortical columns operate on the sub-millisecond temporal and millimeter spatial scale. The study of brain networks, both in healthy and unwell individuals, may reveal new methodologies of treatment or management for disease and injury, as well as contribute to our scientific understanding of how the brain works.

ACKNOWLEDGEMENTS

I would like to thank Dr. Greger for the years we have worked together, for the sometimes-late days and meetings we have spent talking about science and philosophy. Dr. Greger has been most patient, kind, and optimistic during these years.

I would like to thank Dr. P. David Adelson for taking the time away from Phoenix Children's Hospital to help advise on these projects and bring a much-needed clinical perspective to the science. He has always asked about the greater picture, looking at both the scientific merits and potential health care applications of our research.

Dr. Steve Helms Tillery, Dr. Marco Santello, and Dr. Antonia Papandreou-Suppapola have each contributed their time to offer advice and their own expertise to ensure my research is of the highest quality.

Dr. Jeffery Kleim graciously volunteered last minute to join my supervisory committee.

Dr. Francisco Ponce and Dr. Zaman Merzadeh have graciously worked as our collaborators in their positions as neurosurgeons. Without their help, the research presented here could not have been done.

Finally, to my family, who have always been my largest supporters and champions. Without your guidance and parental encouragement, I would not be the man I am today. I always hope to make you proud and I cannot wait to see what life has in store for me in the next chapter.

TABLE OF CONTENTS

Page

LIST OF TABLES

Table Page

LIST OF FIGURES

Figure Page

CHAPTER 1

SIGNALS OF THE BRAIN

Sources of Action Potentials and Local Field Potentials

There are two primary signals involved in neural computation; action potentials (APs) and local field potentials (LFPs). Neurons are specialized cells whose function is to gather, integrate, and transmit signals to facilitate decision making, sensory processing, and behavior.

LFPs are the electrical potential generated from the integration and summation of intracortical extracellular potentials from post-synaptic potentials from neuron activity [1]–[6]. Because LFPs are a summation of many sources, synchronized oscillations will constructively add to produce larger contributions than asynchronous oscillations [5], [7], [8]. The populations of neurons that give rise to LFP will express transient spatial and temporal correlations that will be reflected in the dynamics of an LFP signal. These correlated populations of neurons have been shown to organize in cortical columns with diameters of several hundred microns, though the size of the cortical column varies across cortex [9]–[13]. Cortical columns may be the fundamental computation units of cortical information processing. Activity within a cortical column, or the integration of activity between several cortical columns, may be the source of LFP signals.

The spatial extent of LFPs have been characterized by many studies to range from a few hundred microns to a millimeter or more [3], [14]–[21]. These studies and others suggest that LFPs can contain informative features at the millimeter spatial and millisecond temporal scales and that these signals can be recorded from microelectrodes [22]–[24]. Such signals can be used for fundamental neuroscience, brain-computer

interfaces (BCI), disease diagnostics, and prosthetic applications [25]–[28]. It is of historical interest that the basic design of ECoG electrode grids instantiated in the 1950s has changed little since that time [29], [30], although more recent developments are incorporating microelectrodes in research applications with a focus toward patient care [31], [32].

Recording Functional Connectivity

Functional connectivity is a broad term used to encapsulate different levels of abstractness of the functional relationship between brain areas. Anatomical connectivity studies the physical connections between functionally related brain areas by tracing neuron tracts. More recently, diffusion tensor imaging (DTI) studies the properties of water diffusion through neural tissue in the brain [33]. Highly anisotropic diffusion suggests the presence of white matter tracts. By tracing these tracts, DTI can reconstruct estimations of the anatomical connections of the whole brain.

Most functional connectivity studies use either indirect measures of cortical function such as fMRI [34]–[38] or are spatially imprecise such as electroencephalography (EEG) or macro-electrocorticography (macro-ECoG) [39], [40]. The strength of fMRI is its ability to non-invasively image the entire brain at a millimeter spatial scale. However, fMRI is analyzing the blood-oxygen level dependent (BOLD) signal, which is correlated with increased metabolic activity of neural tissue, but this signal and fMRI in general, lack the ability to interrogate the millisecond level temporal dynamics of neural processing.

Complex network dynamics mediate information processing in the brain between anatomically local (intra-cortical areas) and distant (between distinct cortical and subcortical areas) regions. Electrophysiological functional connectivity is the most direct and concrete method to date to study the underlying neuromechanisms of brain function. This electrophysiological functional connectivity describes the temporal correlations between neurophysiological events (LFP / AP) that are spatially remote, without regard to anatomical connectivity that may or may not be apparent between them.

The correlation between neighboring macroelectrodes, such as EEG or macro-ECoG, falls off slowly with distance [41]. This slow decrease in correlation with distance suggests that macroelectrodes are spatially integrating LFP signals within 1-2 cm of the macroelectrode. However, LFPs have been shown to have spatial scales in the millimeter range [3], [14]–[21], [42]. Millimeter scale LFP signals may be masked by the integration of broader LFP synchronizations.

Presently, a reasonable method for analyzing the electrophysiological functional connectivity of micro-scale networks in and between brain regions are subdurally implanted microelectrodes. Intra-cranial microelectrodes have been successful in several human and animal research for movement and visual processing [3], [10], [20], [26], [43]–[45] . These penetrating and non-penetrating electrodes can record the brain signals at the spatial and temporal scales of neural activity [41]. These electrodes have diameters on the order of ~40 μm – 100 μm. Consequently, their listening radius are ~1 – 2 mm of cortex [41] which is on the scale of a few cortical columns [9], [30]. Neural recordings matching the cortical columnar scale of computation in the cerebral cortex and the spatial scale of LFP may best reveal fine-scale detail of neural processing. Therefore,

microelectrodes are a sensible method to study the behavior and dynamics of neural networks at the same scales they operate.

Cortico-Basal Ganglia Loop

The cortico-basal ganglia loop is currently seen as an organized circuit where the activation of particular networks depends on the specific context and circumstances happening elsewhere in the brain. Early works starting in the 1980's have detailed the pathophysiological model of movement disorders [46]–[48]. Since then others have expanded and discussed the limitations of the original models [49]–[52]. Other works have described the somatotopic organization [53]–[56] and the topographic organization of the cortico-basal ganglia circuit[57]–[62].

Most focus of cortico-basal ganglia loop research is in the motor circuit. This is due the motor deficits exhibiting more pronounced symptoms in disease or injury conditions. Other deficits can be present [57]–[62], such as learning, memory, emotional control, and cognition. However, it is more difficult to design research approaches and therapies for these non-motor deficits. It is interesting to note that these other non-motor aspects may be impacted with the presentation of Parkinson's disease.

The cortico-basal ganglia motor circuit involves five subcortical components in the network: striatum, globus pallidus pars externa (GPe), globus pallidus pars interna (GPi), subthalamic nucleus (STN), and substantia nigra pars compacta (SNR). The circuit (figure 1.1) begins in the motor cortices and with projections to the striatum and STN [63]–[66]. The output nucleus of the basal ganglia is the GPi. A monosynaptic pathway projects from the striatum to the GPi; the direct pathway. A trisynaptic pathway from the

striatum projects first through the GPe, the STN, and then to the GPi; the indirect pathway. Cortical projections through the stratum and STN induce opposite (inhibitory/excitatory) responses in the GPi. Activity in the GPe appear to modulate and

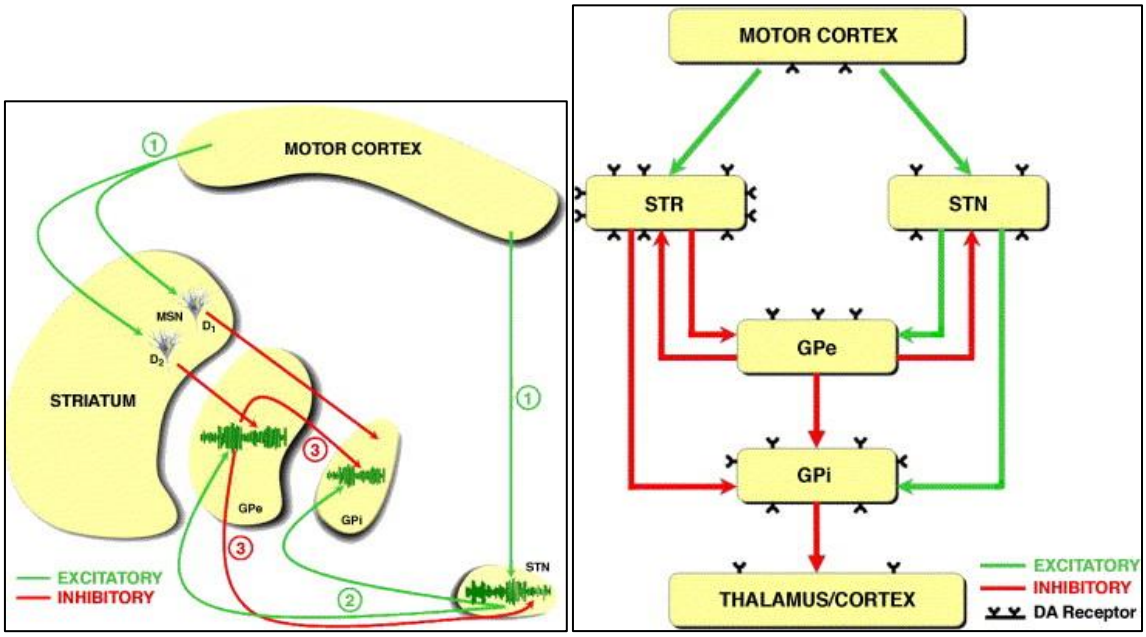

Figure 1.1. Functional organization of the basal ganglia. Left) Anatomical layout. Right) Hierarchical layout. Input from the cortex arrives at the subthalamic nucleus (STN), and the globus pallidus pars externa (GPe) through the medium spiny neurons projections from the striatum (STR). These cortical projections produce opposite (inhibitory/excitatory) disynaptic effect on globus pallidus pars interna (GPi). The GPe modulates the activity back to the striatum and STN through inhibitory, reciprocal projections. The GPi projects to the cortex through the thalamus. All components of the basal ganglia have dopamine receptors and their function is affected by the loss of dopaminergic cells from the SNR in Parkinson's disease. Images reproduced from Obeso et al., Experimental Neurology 2006; 202:1–7.

regulate the connection between the striatum and STN with the GPi through reciprocal inhibitory projections.

Parkinson's disease is a degenerative neurological disorder afflicting the motor system, associated with impairments such as bradykinesia, tremor, and impaired balance. The exact mechanisms causing these symptoms are unknown [67], but their progression is associated with the loss of dopaminergic cells in the SNR. All components of the basal ganglia have dopamine receptors, but the loss of these cells particularly causes an imbalance in the coordination of the direct and indirect pathways as these pathways are inhibited or excited with the loss of dopamine, respectively [48], [50], [68], [69]. This pathological imbalance could interrupt the selection and inhibition of voluntary movements resulting in the movement impairments associated with Parkinson's disease; tremor, bradykinesia, rigidity, and a decline in postural and balance control [67], [69].

Several pathological oscillations of neural signals are associated with Parkinson's disease. Upon reduction of dopamine production a dysregulation of beta-band (12-30 Hz) oscillations appears in cortex; beta-band suppression becomes more difficult during movement [70], [71] and between the cortex and basal ganglia [72]. Patients with Parkinson's disease also exhibit prominent activity within STN in the beta band, which attenuates with dopaminergic treatment, while STN activity in the gamma (60-80 Hz) and theta (4-8 Hz) bands may increase. High-frequency oscillations (HFO, ~300 Hz) initially diminish with treatment, but can recover within minutes in a higher frequency range and with a broader distribution [73].

Aberrant phase-amplitude coupling has also been observed in the Parkinsonian state between beta and gamma bands in deep basal ganglia structures and the primary

motor cortex [74]. In the healthy state, M1 broadband gamma activity displays phase modulation with low-frequency signals in a dynamic, task and site-specific manner. By contrast, excessive Parkinsonian phase-amplitude coupling may restrict the cortex to monotonous activity patterns that may disrupt its ability to respond to signals from other brain areas. This model possibly provides a basis for akinesia, a chief clinical sign of Parkinson's disease.

Dopaminergic therapy with dopamine precursors (levodopa, L-Dopa) is a gold standard for the treatment of Parkinson's disease. However, due to the therapeutic window, side effects of chronic therapy can leave patients cycling between phases of dyskinesia and depression following phases of alert activity [75], [76]. Descriptions of this phenomenon have existed since the earliest studies of levodopa in 1969 [77]. Following the diurnal cycles, these symptoms are strongest in the morning, but can also transition between extremes in cycles of three hours [75].

As Parkinson's disease progresses patients can become eligible for an intra-cranial deep brain stimulator (DBS) which electrically modulated the brain to rescue parkinsonian motor symptoms. Common targets for DBS intervention are the GPi and STN. Debate on the mechanisms of DBS and how it interfaces with the cortico-basal ganglia loop has existed since the 1980s [78]. However, some studies have shown that DBS intervention activates axons and inhibits neuronal cell bodies [79]. Understanding the functional connectivity between basal ganglia and the cortex may lead to more targeted manipulations of cortico-basal ganglia circuitry with DBS.

Speech Production

Speech and language are fundamental to the human experience and concurrently activate multiple brain areas [80], [81]. Prior to modern imaging and sensing technologies, the neural model of language involved the study of speech impairments caused by brain damage. The most notable of these studies are from Broca, Wernicke, Lichtheim, and Gerschwind [82]–[85].

The process of generating lexical phonological representations (speech production) primarily involves two areas: the posterior superior temporal gyrus (pSTG) which is putatively Wernicke's area [82], [86]–[88], and Broca's area, specifically the left pars opercularis (LpOp), a region within Broadmann area 44 [84], [88]–[90]. These two areas of the brain are connected via the arcuate fasciculus, a white matter tract between the temporal and frontal lobes that connects Wernicke's area (phonologic components of language) and Broca's area (motor control for speech production) [91], [92].

LpOp has been identified as a critical component of syllable motor programming, particularly auditory expectation, and constitutes a part of the Broca's area [93]–[95]. LpOp is activated in both covert (silent) and overt (out loud) speech [88], [94], [96] and seems to be segregated into a ventral and dorsal areas with distinct components. The dorsal region of LpOp appears to be involved with phonological encoding (assembling syllables) [88], [94] and the ventral region of LpOp spears to be involved with translation between phonemic and articulatory representations (encoding syllables to orofacial motor programs) [34], [87], [94]. These findings happen to mirror the ventral and dorsal stream hypothesis of speech production [87].

Through anatomical lesion and functional imaging studies, the pSTG, putative Wernicke's area, appears to be involved in speech comprehension [88], [97]–[102]. Such involvement would match the observations that individuals with conduction aphasia or primary progressive aphasia. Both disorders leave individuals with intact auditory comprehension, but speech production develops paraphasic errors. These individuals can hear, comprehend, and follow directions as a healthy individual, but when asked to repeat a phrase the response can be stilted or have transposed sounds. For example, when asked to repeat "bagger" the subject may respond with "gabber"[103], or "seventy-nine" becomes "ninety-seven" [104]. Subjects are aware of these errors and may have difficulty correcting them. Conduction aphasia occurs when the arcuate fasciculus is damaged, resulting in disruption to the auditory-motor integration system [91], [105]. Primary progressive aphasia, causes degeneration of cortical tissue focused on the inferior parietal and posterior superior temporal region [106], [107]. Somewhat confusingly, Wernicke's aphasia, or receptive aphasia, is a similar disorder but presents in deficits of language comprehension [82]. This aphasia most commonly occurs after a stroke, when the damage accrues in the cortex just posterior to primary auditory cortex and anterior to Wernick's area. An individual with this disorder can speak fluently, effortlessly, and with prosody, but the sentences are meaningless. Patients often are unaware of their deficits. Lesion to the cortex in STG, just anterior to pSTG, can is associated with receptive aphasia [34], [102], [104], [108], [109].

CHAPTER 2

ELECTROPHYSIOLOGICAL FUNCTIONAL CONNECTIVITY IN MICRO-SCALE CORTICAL-SUBCORTICAL NETWORKS IN PATIENTS WITH PARKINSON'S DISEASE

Abstract

Parkinson's Disease is associated with the disruption of normal function in cortico-basal ganglia loops, leading to various movement impairments. Electrophysiological recordings taken using macro-ECoG electrodes have shown excessive coupling between cortical regions and subcortical structures, such as between beta and gamma bands in deep basal ganglia structures and the primary motor [74]. Recordings taken using micro-electrocorticography (micro-ECoG) electrodes may potentially characterize patterns of functional connectivity, or temporal correlations between spatially remote neurophysiological events, at a finer spatial scale. This study used micro-ECoG arrays and penetrating FHC microelectrodes to investigate millimeter-scale functional connectivity between basal ganglia neurons and areas of premotor cortex in patients with Parkinson's Disease. In addition to analysis of five classical local field potential (LFP) bands (Theta, Alpha, Beta, Gamma, and Chi), this study sought to detect patterns of functional connectivity in a high-frequency (250-2000 Hz) range matching the peaks in frequency content of action potential waveforms. 83 of 127 subcortical neurons were found to express significant correlations with cortical LFP power dynamics. 12 of the 83 neurons were coupled to multiple cortical LFP frequency bands. This result may imply that some neurons express frequency-domain multiplexing and may be embedded in multiple cortico-subcortical networks. These dynamics may subserve information

exchange between these structures. This approach may lead to further insight into the micro-scale network dynamics underlying cortico-basal ganglia-cortico function in both healthy and disease states.

Introduction

Parkinson's Disease is a degenerative neurological disorder afflicting the motor system, associated with impairments such as bradykinesia, tremor, and impaired balance. The exact mechanisms causing these symptoms are unknown [67], but their progression is associated with the loss of dopaminergic cells in the Substantia Nigra. Parkinson's Disease is implicated in the disruption of normal function of the basal ganglia in the cortico-basal ganglia loop [68]. The basal ganglia are a system of subcortical nuclei situated at the base of the forebrain that form multiple parallel modulatory feedback loops with many wide areas of the cerebral cortex. These feedback systems may contribute to movement selection, initiation, amplitude, and termination, as well as motor learning and the reward system of the brain [69]. Parkinson's disease is thought to be caused by the depletion of dopamine producing cells of the substantia nigra, resulting in erroneous activity in the direct and indirect pathway model of the cortico-basal ganglia loop [67], [69]. A current hypothesis is that the movement impairments associated with PD (tremor, bradykinesia, rigidity, and a decline in postural and balance control) occur due to the interruption of the selection and inhibition of voluntary movements [69].

Several pathological oscillations of neural signals are associated with Parkinson's disease. Upon reduction of dopamine production, the cortex experiences dysregulation of

beta-band (12-30 Hz) oscillations [70], [71] and between the cortex and basal ganglia [72]. Patients with Parkinson's disease also exhibit prominent activity within STN in the beta-band, which attenuates with dopaminergic treatment, while STN activity in the gamma (60-80 Hz) and theta (4-8 Hz) bands may increase. High-frequency oscillations (HFO, ~300 Hz) initially diminish with treatment, but can recover within minutes in a higher frequency range and with a broader distribution [73]. Dopaminergic therapy frees these HFOs from beta-band coupling [73]. Once decoupled, the HFO amplitude modulates with movement. Synchronization between neuronal action potential firing in STN and cortical field potentials recorded from primary motor cortex (M1) using macro-ECoG electrodes [110]. Aberrant phase-amplitude coupling has also been observed in the Parkinsonian state between beta and gamma bands in deep basal ganglia structures and the primary motor cortex [74].

Electrophysiological functional connectivity describes the temporal correlations between neurophysiological events that are spatially remote, regardless of any physical or anatomical connectivity that may or may not be apparent between them. The functional relationships between neural activity in basal ganglia structures and cortical neuronal populations may potentially be more precisely characterized through more localized and specific surface recordings. Neural recordings matching the cortical columnar scale of computation in the cerebral cortex may help identify new patterns of aberrant neuronal activity among different, smaller functionally coupled regions of the brain. The aforementioned studies of cortico-basal ganglia synchronization typically recorded surface potentials from macro-scale, clinical ECoG grids, whose electrodes are millimeters in size and detect the aggregate activity of large neuronal populations. In

contrast, micro-ECoG arrays allow analysis of local field potential (LFP) signals at a millimeter to sub-mm scale, closer to the cortical columnar scale [41]. This study employed micro-ECoG arrays and penetrating FHC microelectrodes to investigate relationships between premotor cortical neuronal population activity and single neurons in basal ganglia in patients with Parkinson's disease. The spike-triggered average (STA) of LFP signals is one method of detecting functional connectivity, assessing the strength of postsynaptic activity in a cortical region potentially affected by spiking in a different location [111]–[113].

The AP-band (250-2000 Hz) has been hypothesized to include components of firing from nearby neurons, including neurons too distant from the microelectrode to have resolvable waveforms [113]. Purpose-built surface micro-electrodes with diameters as small as 10 μm have been used to detect and isolate waveforms of individual action potentials from superficial cortical neurons [114]. As the micro-ECoG arrays record on the spatial scale of cortical columns, synchronous neural activity within the columns may register in the neural recording. It is thus likely that the micro-ECoG arrays in this study may record the high frequency bands corresponding to spectral peaks of action potential waveforms. This study used STAs between single neurons in basal ganglia and cortical micro-ECoG recordings to investigate functional connections. The ability to detect features of functional connections using non-penetrating surface electrodes could be particularly useful in clinical applications and research involving human subjects.

Methods

Experimental subjects were parkinsonian patients undergoing anesthetized bilateral DBS implant surgery. Burr holes were drilled over the dorsal frontal lobe. A 4x4 micro-ECoG array (1 mm spacing and 75 um diameter, PMT Neurosurgical, Chanhassen, MN) (Figure 2.1) was slid epicortically to lie on motor association cortex, posterior to the coronal suture. A subcortical microelectrode (FHC, Bowdoin, ME) was ipsilaterally inserted through a cannula and descended through the therapeutic target tracks, pausing at subcortical structures to record neuronal activity. The subcortical microelectrode was then removed, and the therapeutic electrode was implanted along the same track.

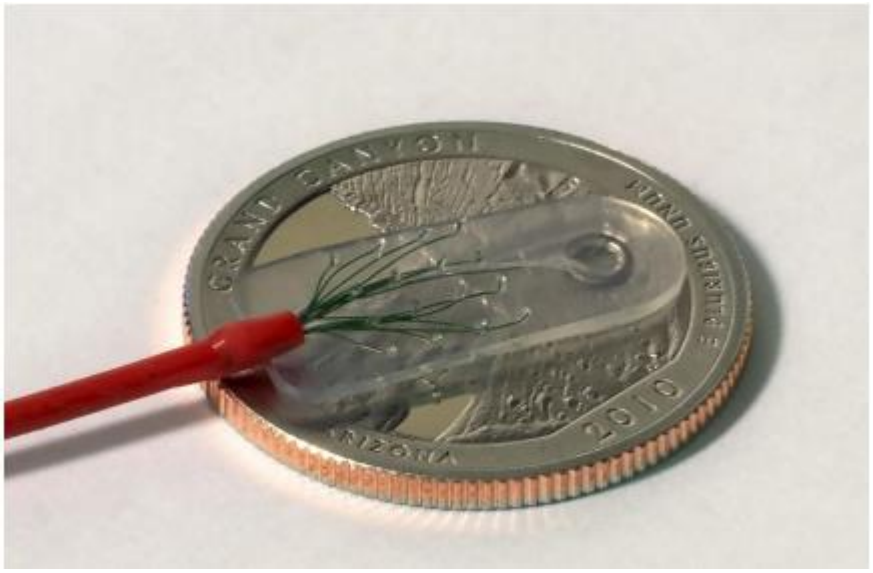

Figure 2.1. PMT Cortical micro-ECoG array. The cortical micro-ECoG array is shown next to a United States quarter for scale. Electrodes are 75 µm in diameter and have 1 mm spacing. The larger electrode disc towards the right is a reference electrode.

Subjects

All subjects were volunteers undergoing standard clinical DBS implantation at Barrow Neurological Institute (Phoenix, AZ) (Table 2.1).

Equipment and Recording

The cortical micro-ECoG array and the subcortical microelectrode were recorded at 24.4 kHz with a data acquisition system (Tucker-Davis Technologies, Alachua, FL).

During the intraoperative session, the penetrating microelectrode would be manually descended until a neuron was recorded. At each pause of the descent, markers for the depth of the microelectrode and the corresponding basal ganglia structure were manually added to the recording file. Marker data were encoded as 8-bit ASCII characters. The Tucker-Davis Technologies (TDT) digital input only recorded voltage values when a change was detected. To avoid problems where duplicate characters were not recorded, every other ASCII code was increased by a value of 128. When extracted into MATLAB, all marker stream values above 127 had their ASCII value decreased by 128. Then, the marker stream was converted into a text string. Asterisk characters denote delimiters for splitting the text string. The timestamp of each asterisk indicates when that text segment was delivered to the TDT system.

Table 2.1

Patient Demographics

Subject	Age	Sex	Target Structure	Implantation	Years Diagnosed	Recorded Hemisphere
2016PB01	62	M	STN	Bilateral	4	Right
2016PB02	65	M	STN	Bilateral	12	Left
2016PB04	66	F	GPi	Bilateral	10	Right
2016PB05	65	M	STN	Bilateral	6	Right
2016PB06	67	M	STN	Bilateral	6	Right
2017PB01	55	M	STN	Bilateral	7	Right
2017PB02	55	M	GPi	Bilateral	15	Right
2017PB03	62	M	GPi	Bilateral	14	Right

Data Analysis

All analysis was completed in MATLAB (The MathWorks, Inc., Natick, MA).

Cortical LFP Filtering

Each cortical recording was first lowpass filtered to 2400 Hz using a 9^{th} order Butterworth filter and then down sampled to 4800 Hz. 60 Hz line noise and harmonics were filtered using 3^{rd} order Butterworth notch filters. This down sampled data was then filtered with an 8^{th} order Butterworth filter (20dB stop band attenuation) for five of our frequencies of interest: Theta (4-7 Hz), Alpha (8-15 Hz), Beta (16-30 Hz), Gamma (31-80 Hz), Chi (81-160 Hz). The cutoff frequencies were one Hz less and greater than the given band range. AP-band (250-2000 Hz) was highpass filtered with an 8^{th} order Butterworth filter with a 250 Hz pass band and 160 Hz cutoff frequency (60 dB stop band attenuation).

AP Isolation and Sorting

The subcortical microelectrode recordings were highpass filtered using a Butterworth filter to isolate action potential waveforms (Cutoff at 160 Hz, passband at 200 Hz, stopband attenuation 60 dB). Positive and negative voltage spikes beyond 3 times the RMS value of the recording were extracted into snippets as candidate action potentials. Candidate snippets were projected into principal component space using the top three principal components. Initial sorting of AP waveforms from neurons at each subcortical recording depth was performed using an automated algorithm based on mixtures of multivariate t-distributions [115]. Cluster grouping and separation was adjusted from the automated process by manual visual inspection of the clusters and their cluster ellipsoids (centered at the cluster centroid and radii of 1.96 standard deviation) in PCA space, the inter-spike interval distributions, spike locations in the voltage time series recording and the collective experience of the researchers conducting the study.

Spike Triggered Average

For each isolated subcortical neuron, the spike-triggered average of the surface local field potential was computed for every electrode on the micro-ECoG array from -0.5 to +0.5 seconds relative to subcortical spike times. Cortical micro-ECoG electrode 1 was excluded from analysis due to miswiring of a cable causing electrode 1 to instead record the data from the penetrating microelectrode.

STAs were gathered from each of the studied frequency bands.

Resampled and Surrogate Data Generation

For each subcortical neuron, the spike times were resampled with a bootstrap method 500 times. In each resampling, a random 25% of spike times were dropped out. The resampled STA was then calculated using these resampled spike times.

To generate surrogate baseline data for statistical analysis, surrogate spike times were generated by randomly jittering the spike times between 0-0.5 seconds. This process disrupts temporal correlations between the subcortical neuron and the cortical LFP. This procedure was performed in a bootstrap resampling manner 500 times with a 25% dropout for each surrogate. A surrogate STA was computed using each of these surrogate spike times.

Resampled and surrogate STAs were computed for each neuron and each frequency band. A total 762 (127 neurons * 6 frequency bands) resampling procedures and 762 surrogate procedures were performed.

STA Analysis

For each of the resampled and surrogate STA waveforms instantaneous mean spectral power was computed for six frequency bands. To perform this analysis, multi-taper power spectral density estimates (Chronux toolbox) were computed from the spike-triggered averages using 0.25 s windows, padding to the next highest power of 2, 80 Hz sampling rates, and a single taper to maximize the frequency resolution. The single taper is similar to a Hanning window, but the choice to use a multi-taper computation allowed us to test other configurations.

The resulting time-frequency matrices were normalized across frequencies with respect to the average spectrum in order to minimize masking of low amplitude, high frequency signals by higher amplitude, lower frequency signals in each frequency band. Subsets of the resulting normalized time-frequency matrices corresponding to each frequency band were extracted and averaged over frequency bins to create a time-varying index of spike-triggered average spectral power for each frequency band, electrode, and resampling iteration.

For each frequency band, to determine if the spike-triggered average spectral power was different from the surrogate baseline, the resampled spike-triggered average spectral power vectors made from true spike times were projected into principal component space along with the STA vectors made from surrogate spike times. The first three principal components were used in this projection. Ellipsoids with radii of 1.96 standard deviations from the centroid were generated for each STA cluster. The two clusters were considered significantly separable if their ellipsoids did not intersect. The STAs that differ significantly from the surrogate data may represent that the subcortical neuron is functionally connected to the cortex for that channel and frequency band. Since LFPs are the summation and integration of postsynaptic potentials from neural activity, the subcortical neuron may be functionally connected to small populations of cortical neurons whose activity is oscillating in a frequency band. An example of ellipsoid separation is seen in Figure 2.6.

Table 2.2

Total number of subcortical recordings and total number of neurons isolated from those recordings, by subcortical structure.

	AT	STN	SNr	GPe	GPi	Total
Subcortical recordings	3	32	5	15	18	73 Locations
Isolated neurons	7	54	14	19	33	127 Neurons

Table 2.3

Number of isolated subcortical neurons for each subject and subcortical structure.

Subject	AT	STN	SNr	GPe	GPi	Total
2016PB01		2	6			8
2016PB02	6	14	6			26
2016PB04				12	15	27
2016PB05		12				12
2016PB06		16	2			18
2017PB01	1	10				11
2017PB02					2	2
2017PB03				7	16	23
Total	7	54	14	19	33	127

Results

Eight patients underwent a standard clinical bilateral DBS implanting procedure with either STN or GPi therapeutic targets. The microelectrode followed a standard clinical trajectory into the brain. When the STN was the target, the surgical tract passed through anterior thalamus (AT), subthalamic nucleus (STN), and SNr. When GPi was the target the surgical tract passed through the external and inter parts of globus pallidus (GPe and GPi).

In total, action potential waveforms from 127 neurons were isolated from 73 recording locations across 5 basal ganglia structures in 8 Parkinsonian patients undergoing standard clinical bilateral DBS implant surgery (Table 2.1, 2.2, 2.3). The results of the spike sorting process are shown for an example recording depth with 3 neurons in figure 2.3. Isolated neurons had AP counts ranging between 78 to 8,493 APs.

Increased modulation in amplitude compared to surrogate data could be seen in the spike-triggered average LFP power (example figure 2.4, 2.7) as well as their corresponding frequency-normalized spectrograms and frequency band-averaged instantaneous spectral power vectors (example figure 2.5). Of the 127 neurons isolated in this study 83 (65%) were found to be correlated with cortical LFP modulation in any frequency; 12 (9.4%) subcortical neurons were correlated with cortical theta-band modulations, 11 (8.7%) neurons were correlated with alpha-band, 5 (3.9%) neurons were correlated with beta-band, 6 (4.7%) neurons were correlated with gamma-band, 19 (15%) neurons were correlated with chi-band, and 42 (33%) neurons were correlated with AP-band (Table, 2.4).

The example data in figure 2.7 are reflective of the general trends observed in Alpha-band and in AP-band across patients and basal ganglia structures (Figure 2.8): increases in cortical alpha-band power tended to lead subcortical spike times (mode peak latency of = -40 ms), while cortical power in AP-band tended to lag subcortical spike times (mode peak latency = +50 ms) (Figure 2.8).

A total of 356 (18.7 %) significant spike-triggered average functional couplings were observed between subcortical neurons and activity in AP-band from cortical surface electrodes, roughly one order of magnitude more than observed in the next closest

frequency range, Alpha-band with 34. Table 2.5 summarizes the number of significant functional couplings found by basal ganglia structure and frequency band.

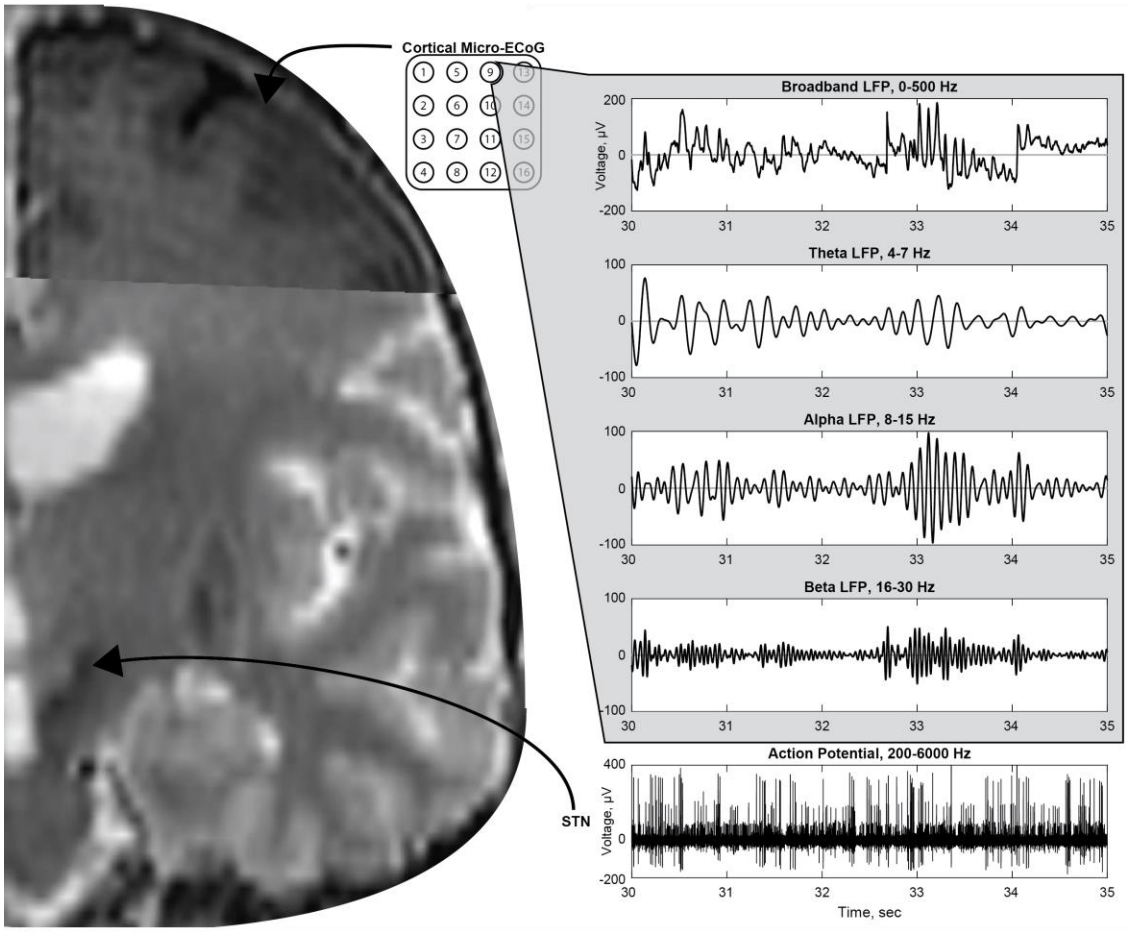

Figure 2.2. Data sources. Left, merged MRI and CT images. Top right, cortical LFP signals from channel 9 of the micro-ECoG array of subject 2016PB02 separated into broadband, theta band, alpha band, and beta band. Bottom right, bandpass filtered action potential data from the STN.

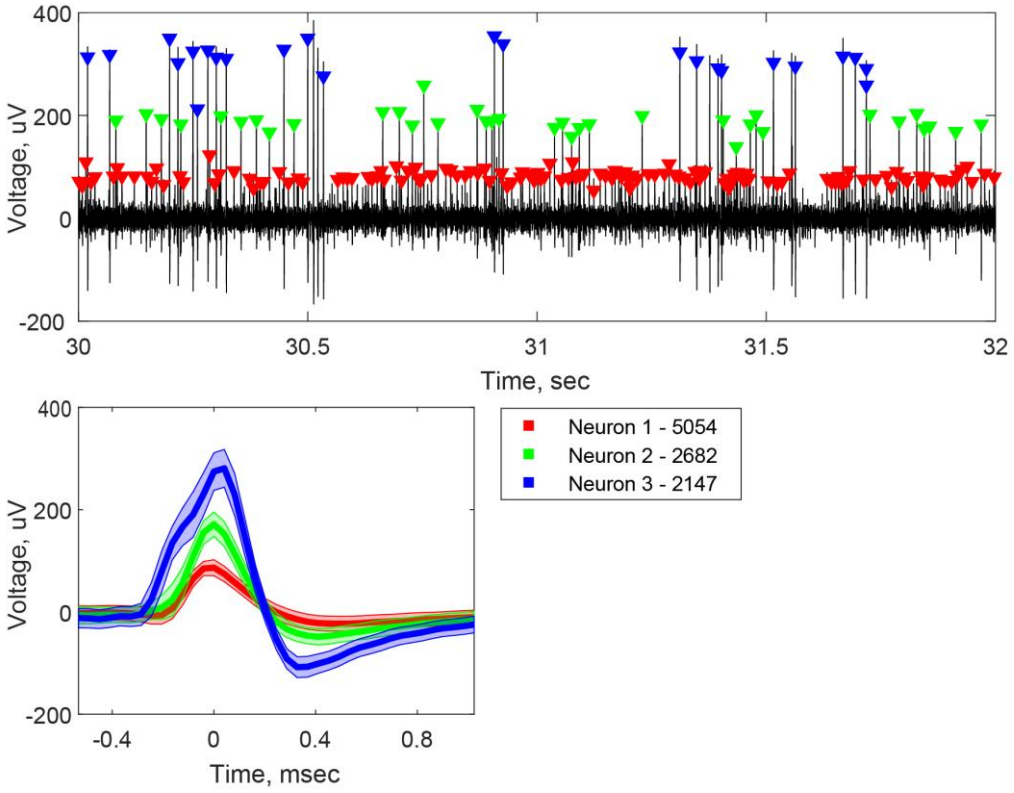

Figure 2.3. Example AP isolation. Top) Two second clip from the STN from subject 2016PB02. Three neurons were isolated during the two-minute recording. Bottom) AP waveforms for each neuron (+/- 1 standard deviation).

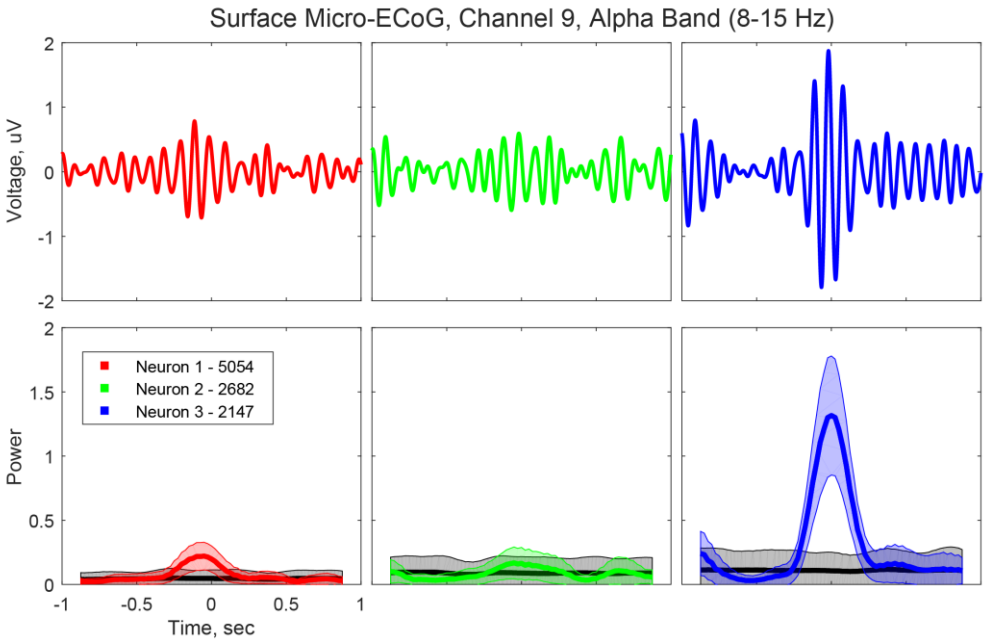

Figure 2.4. STA LFP and STA LFP Power. Top row) 2 second clips of alpha band AP-triggered LFP averages from three STN neurons (Figure 2) in subject 2016PB02. Bottom row) Resampled (color) and time shifted (black) AP-triggered LFP power (+/- 2 standard deviation).

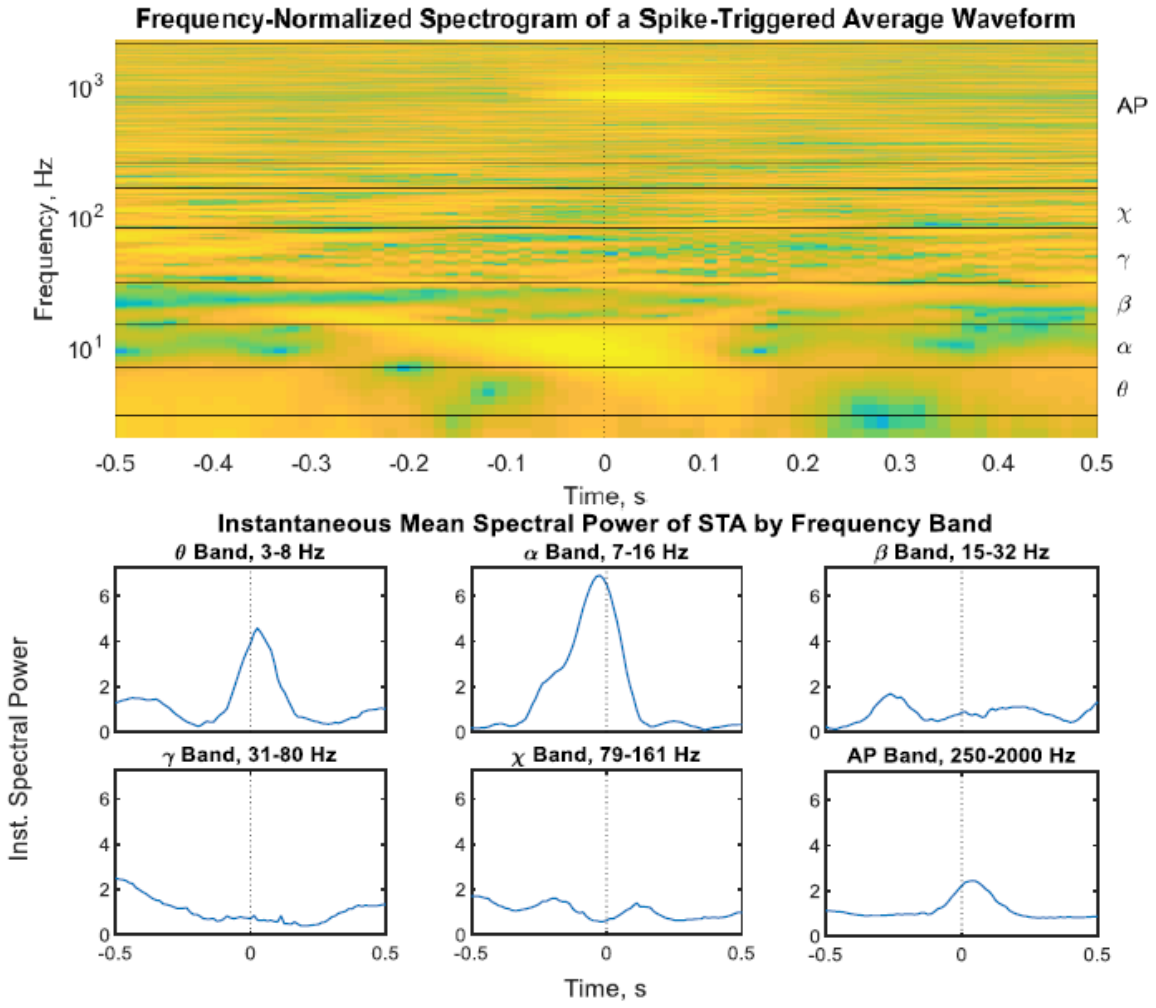

Figure 2.5. STA Spectral Power by Frequency Band. Top, a frequency-normalized spectrogram of the example neuron 3 (Figure 2.3) shows the six frequency bands for which instantaneous mean spectral power was computed. Spike time is indicated by the dotted black line at t = 0, while horizontal solid black lines indicate boundaries of frequency bands. Frequency is plotted on a logarithmic scale to facilitate viewing of all frequency bands together. Increases in spectral power relative to subcortical spike time can be seen in alpha-band and the high frequency band potentially associated with action potential spectra, AP-band. Bottom, instantaneous mean spectral power is shown for each of the six frequency bands.

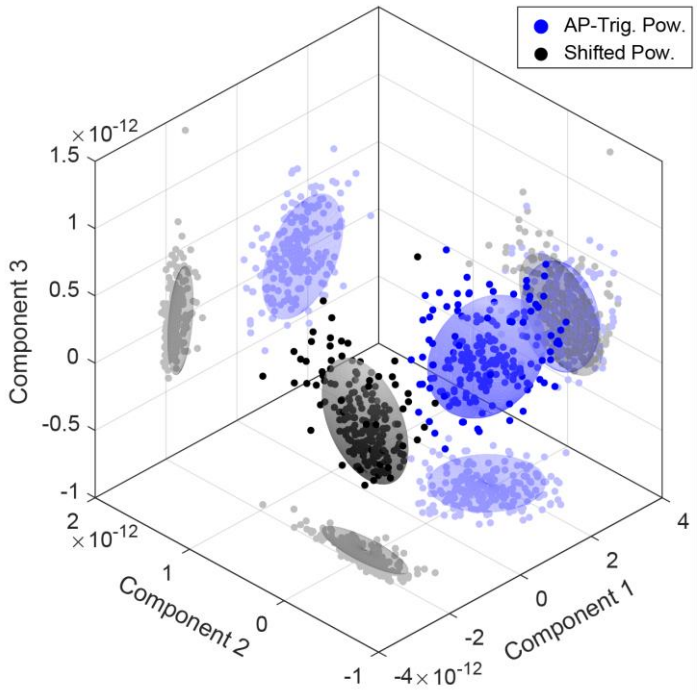

Figure 2.6. PCA projection STA LFP power. The resampled STA alpha band spectral power vectors are projected into Principal Component Space using the first 3 principal components. Ellipsoids are shown at 1.96 standard deviations for the clusters in PCA space from STAs made from true spike times (blue) and from surrogate spike times (black). The STA spectral power from true spike times was classified as significantly different from baseline as the ellipsoids do not intersect.

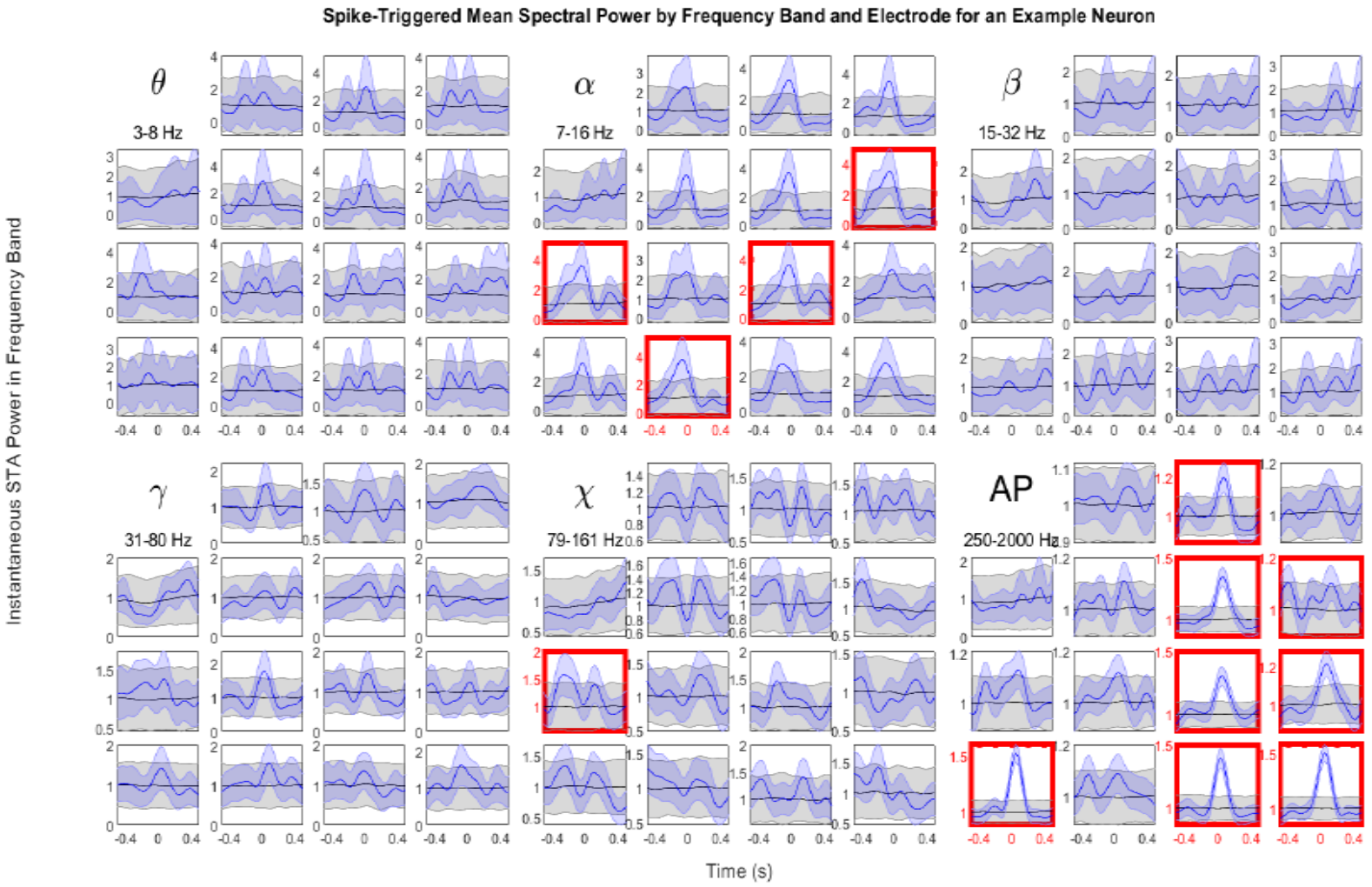
Spike-Triggered Mean Spectral Power by Frequency Band and Electrode for an Example Neuron
θ
3-8 Hz
α
7-16 Hz
β
15-32 Hz
γ
31-80 Hz
χ
79-161 Hz
AP
250-2000 Hz
Instantaneous STA Power in Frequency Band
Time (s)

Figure 2.7. Significantly Coupled STA Spectral Power Means. Data are shown for an example subcortical neuron in STN. Increases in power roughly centered on subcortical spike time can be seen in cortical surface recordings in Alpha-band and the AP-band. Subplots for each frequency band correspond to physical location of electrodes on the surface micro-ECoG array. Blue time series plots represent mean spectral power for spike-triggered averages resampled from true spike times, while black plots represent mean spectral power averaged and resampled from surrogate, jittered spike times. Shaded areas are ± 1.96 standard deviations of the resampled vectors from the mean. Red bolded subplots indicate mean STA spectral power vectors that were significantly different from the surrogate baseline vector, i.e. resampled distributions whose clusters in PCA space did not overlap at 1.96 standard deviations

Table 2.4

Counts of Significant Neurons by Anatomical Structure and Frequency Band

		AT	STN	SNr	GPe	GPi	Total
Total subcortical locations		3	32	5	15	18	73 Locations
Total isolated neurons (Table 1)		7	54	14	19	33	127 Neurons
Subcortical locations correlated with cortical LFP		2	25	3	8	8	55 Locations
Subcortical neurons correlated with cortical LFP		3	42	10	7	11	83 Neurons
Num. neurons correlated by frequency:	Theta	0	9	2	1	0	12
	Alpha	0	10	0	0	1	11
	Beta	0	1	1	1	2	5
	Gamma	0	2	0	1	3	6
	Chi	1	14	1	2	1	19
	AP Band	1	25	3	4	9	42

Top section, subcortical locations and isolated neurons, separated by total number recorded and total number significantly correlated with at least one cortical micro-ECoG electrode, by structure. Bottom section, number of subcortical neurons significantly correlated with at least one cortical micro-ECoG electrode, by frequency and structure.

Table 2.5

Number of comparisons.

Set	Count	Calculation
Neurons	127	
Frequency Bands	6	
Electrodes (Cortical micro-ECoG)	15	
Number of neuron-LFP comparisons within a frequency band	1905	neurons * electrodes
Total number of neuron-LFP comparisons	11430	neurons * electrodes * bands

Total number of comparisons within each frequency band and across all frequency bands. The calculation is included and the inputs come the total number of subcortical neurons, frequency bands analyzed, and micro-ECoG electrodes.

Number of detected spike-triggered average functional couplings.

Frequency Band	Neurons	Num. Sig. Couplings	Avg. Num. Sig. Electrodes Per Neuron
Theta	12	27 (1.4 %)	2.25
Alpha	11	34 (1.7 %)	3.09
Beta	5	6 (0.3 %)	1.20
Gamma	6	8 (0.4 %)	1.33
Chi	19	27 (1.4 %)	1.42
AP Band	42	356 (18.7 %)	8.48
All Bands	83	458 (4.0 %)	5.52

Column 1) Frequency band labels. Column 2) Number of subcortical neurons significantly correlated with at least one cortical micro-ECoG electrode (Table 2.4). Column 3) The number of significant correlations with cortical micro-ECoG electrodes (percentages calculated by dividing by 1905 for individual bands, 11430 for all bands). Column 4) Average number of electrodes each neuron was significantly coupled with (Column 3 divided by Column 2).

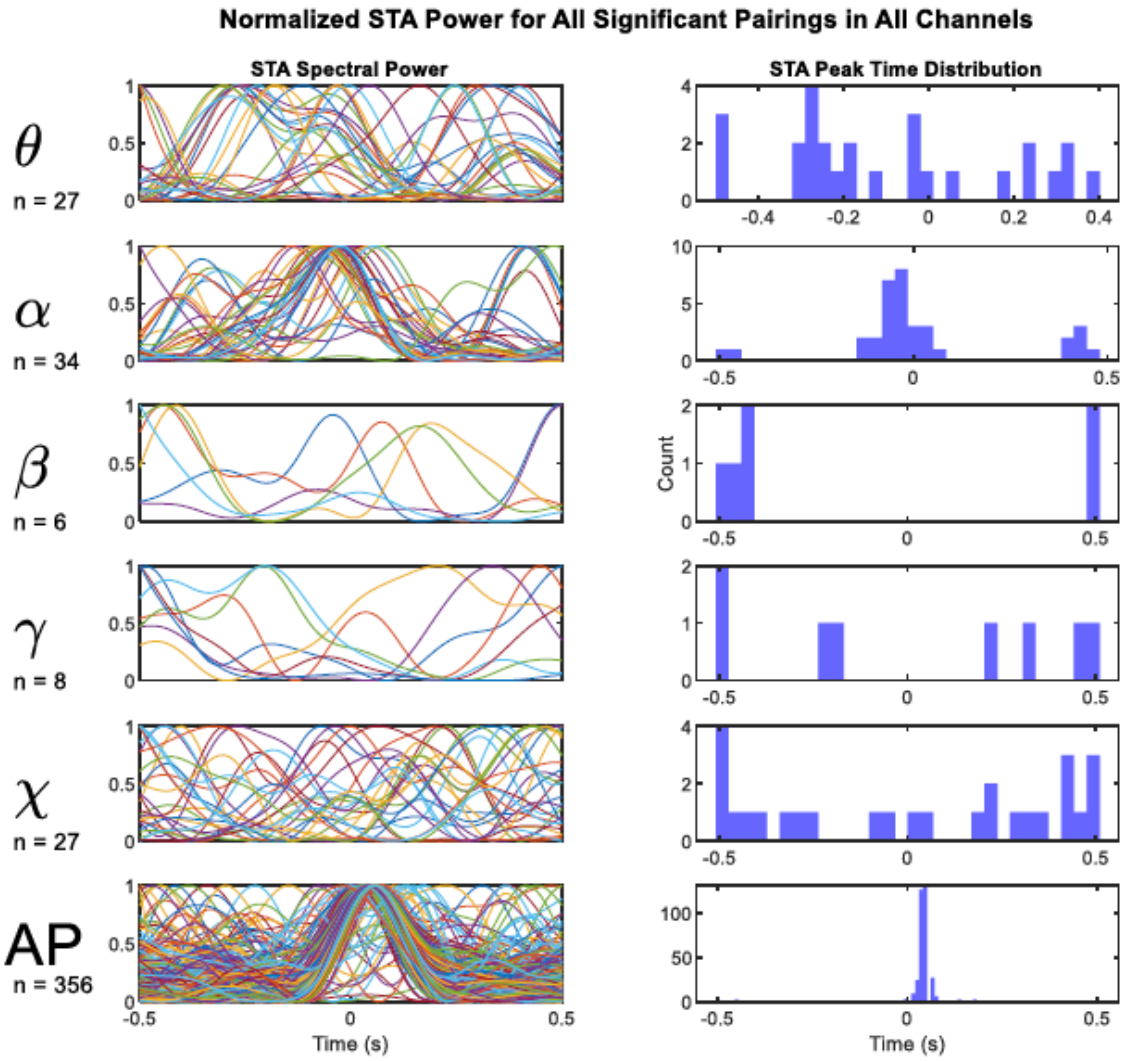

Figure 2.8. Normalized STA Power for All Significant Pairings in all Channels. Across all patients and Basal Ganglia structures, the AP-band (250-2000 Hz) showed significant coupling in 356 pairs of subcortical neuron to cortical surface recordings, out of 1,905 total pairs per frequency band. Alpha-band showed the next greatest amount, at 34 significantly coupled pairs. Increases in STA spectral power had modes of -270 ms relative to subcortical spike time in Theta-band, -40 ms in Alpha-band, and +50 ms in AP-band. Distributions of spectral power increase in Beta, Gamma and Chi-bands did not show a clear central tendency.

Discussion

A total of 458 significant neuron-LFP couplings were detected across all frequencies and electrodes (Table 2.5). This number is only 4% of the total number of neuron-frequency band-electrode comparisons analyzed in this study. Of the 458 significant neuron-LFP couplings 356 of them were observed to be significant coupling between a subcortical neuron and cortical AP-band. The AP-band analysis was responsible for 78% of all detected function connections in this study. This is an order of magnitude higher than the number of significant trends observed in any other frequency band. This discrepancy might be related to fundamental differences between the nature of action potential spiking and the bandlimited synchronous oscillations in LFP signals, and the amplitude reduction induced by the spike-triggered averaging process. LFP waveforms averaged by alignment on spike times inherently undergo large amounts of destructive interference from averaging out-of-phase snippets together, driving the averaged amplitude towards 0. STA waveforms in this study showed amplitudes 2 orders of magnitude lower than raw LFP signals. Similar amplitude reduction has been observed in STA waveforms recorded from penetrating microelectrodes in macaques, and the reduction was noted to increase with increasing LFP frequency and greater distance between electrodes [113]. Phase locking of action potentials to a certain frequency band of the LFP signal results in attenuation of the destructive interference as the spike-centered snippets are overall more synchronous, resulting in greater amplitude of the average waveform in that frequency band relative to spike time. Spike-triggered trends in LFP frequency bands thus reflect patterns in signal phase relative to spike time, and not just patterns in amplitude of the signal in the frequency band.

Action potentials, however, are orders of magnitude shorter-lived than LFP oscillations (commonly on the order of 2 milliseconds for single AP waveforms, vs an approximately 100 ms period for 1 oscillation of Alpha-band) and are effectively only one "cycle" long, as opposed to the continuous oscillations of LFP signals. Signal interference of individual action potential waveforms, destructive or constructive, would require correspondingly tighter temporal alignment of individual spike-centered snippets in order to occur. Additionally, action potential waveforms often exhibit an imbalance in the amplitude of their positive and negative phase [6], which could limit the amount of destructive interference even upon exact temporal alignment of positive and negative phases. It is therefore possible that spike-triggered average waveforms could be less affected by synchrony of continuous oscillations in the AP-band (250-2000 Hz) frequency range compared to the sensitivity of STA waveforms to synchrony of continuous oscillations in other, lower frequency bands. Rather than reflecting synchrony of oscillations between 250-2000 Hz, spike-triggered trends in the AP-band could reflect the total amount of spiking from the local neuronal population, or gross local firing rate.

The spectrograms of cortical surface STAs show frequency localization of the increase in AP-band activity; rather than a broadband increase tapering off from lower frequency bands such as gamma or chi, distinct peaks were typically observed between 800-1600 Hz. Additionally, increases in cortical AP-band activity showed tight temporal coupling relative to subcortical spike times, with a mode lag time of +50 ms across patients and basal ganglia structures, with less variance than observed in lower frequency bands. One possible explanation for the low variance and consistently short lag from subcortical spike to cortical peak in AP-band power is that propagation time of axons,

synaptic neurotransmitter diffusion, and reciprocally coupled neuron recursion time have been observed to be on the order of 10 ms or less [8], [116]–[118]. While far from definitive, the frequency localization and tight temporal coupling of the 250-2000 Hz frequency band are consistent with a possible contribution of action potential waveforms in a local population recorded from the surface electrodes. Rather than representing spike-field coupling, significant coupling in the high frequency band from 250-2000 Hz could instead possibly represent a form of rapid neuron-to-neuron coupling.

Surprisingly, very few significant couplings were observed in Beta-band between subcortical neurons and cortrical field potentials, despite aberrant coupling in beta band being a hallmark of Parkinsonian pathology [71], [119], [120]. One possible explanation could be that anesthesia has been noted to have pronounced effects on brain activity [121], [122]. Anesthesia has been noted to have several effects on functional connectivity in different subcortical and cortical regions. Propofol has been observed in BOLD fMRI studies to reduce functional connectivity between thalamus and cortex, [123]. Biophysical models of neuronal dynamics have indicated that beta oscillations can be generated by the effect of propofol in cortex alone, without necessarily requiring thalamic participation [124]. Anesthesia has been associated with wider synchronization in the brain, particularly in low-frequency rhythms, which have been linked to layer specific pyramidal neurons acting as local pacemakers [125].

Observed functional connections varied on a channel-by-channel basis within any particular frequency (Figure 2.7). These variations indicate that cortical columnar differences between cortical regions just millimeters apart are differentially functionally connected to the spiking of a particular subcortical neuron. These micro-scale spatial

dynamics support the idea the cortex is embedded in multiple overlapping cortico-basal ganglia networks. Additionally, the presence of significant coupling in multiple frequency ranges for a single neuron suggest the presence of parallel networks that are multiplexed in the frequency domain. The findings of multiple, parallel, frequency domain multiplexed networks may be related to recent evidence of thalamic control of functional connectivity within and between cortical regions [126]–[130]. Other studies have noted that pathological rhythms emerge in the parkinsonian state [70]–[72], [129], [131]. It may be that Parkinson's disease and other movement disorders arise from a dysfunction in the regulation of functional connectivity within and between cortical regions and basal ganglia. Such analysis may reveal novel pathways for treatment by externally regulating functional connections via stimulation, instead of creating a virtual lesion in the STN by more conventional therapies [32], [119], [120], [131], [132].

We have validated that microelectrodes can record interesting and potentially useful cortical-subcortical electrophysiological functional connections. However, since the microelectrodes were not consistently localized to the same, specific, area of cortex, the data suggest that the detected cortical-subcortical connections are relatively broad and diffuse throughout motor associated cortex. Since the microelectrodes usually span such a limited amount of space a key consideration for future research will be to precisely place and localize microelectrodes to brain regions that are relevant to the hypothesis being tested.

Limitations

All recordings studied were taken from anesthetized patients. Our findings may reflect the default mode network interactions, rather than cortical-subcortical interactions responsible for the presentation of symptoms. The cortical placement of the micro-ECoG grid was constrained by clinical need, which resulted in placement variations between subjects. All grids were placed on a pre-motor or motor association gyri. We did not study patients while they were taking dopamine replacement therapy, as such therapy is stopped 24 hours before surgery. It is unclear how a therapy like levodopa would affect our observed cortical-subcortical interactions [133]. These patients have been diagnosed with Parkinson's for many years. Consequently, our observations may reflect compensatory changes in the cortical-subcortical circuitry or long-term effects of chronic levodopa therapy [134], instead of the underlying disorder.

Future Work

Future work will focus on perturbing the cortico-subcortical networks by stimulating the STN with a therapeutic stimulator (Medtronic, Minneapolis, Minnesota). An experiment setup similar to the one described above (simultaneous recording of basal ganglia and cortex) will have an additional process of stimulating the contra-lateral STN. This stimulation will take place with four blocks of trials, each block separated by three minutes of baseline with no stimulation. Each block of stimulation consists of 10 trials of 10 seconds on / 10 seconds off stimulation pattern. The stimulation voltage is set to 3 V. The stimulation frequency will be set to one of four frequencies for each block of trials: 140 Hz (within the standard therapeutic range), 20 Hz, 250 Hz, and 70 Hz. We

hypothesize that functional connectivity between a subcortical neuron and cortical LFPs with change when the networks are perturbed with stimulation. Perhaps revealing novel biomarkers useful for adaptive therapeutic stimulation to ameliorate Parkinsonian symptoms.

Additionally, recent research has investigated the dynamics of LFP rhythms [119], [120], [131]. The methods used in this paper are ill-suited to study these LFP power modulations and subsequent analyses may reveal additional functional connections based on the modulation of LFP power, instead of the presented bolus increase in cortical LFP power. The methods described above are ill-suited to exploring rhythm dynamics as the dynamics are averaged out in process of computing the spectrogram. One framework for studying rhythms is to bandpass the broadband LFP data to a desired frequency bin, calculate the envelope of the signal, then compute the spectrum of that envelope. This process may reveal that a particular subcortical neuron is correlated not only with activity in cortical gamma-band, rather, a particular neuron is correlated with a 20 Hz rhythm and a 50 Hz rhythm in gamma-band. Such analysis may lead to a more nuanced understanding that may reveal useful biomarkers for the treatment of disease [32], [119], [120], [131], [132].

CHAPTER 3

NETWORK DYNAMICS IN HUMAN SPEECH PRODUCTION: FORMATION AND TEMPORAL EVOLUTION OF NETWORK CONNECTIONS IN SPEECH AREAS. IMPLICATIONS TOWARD SPEECH REAFFERENCE.

Abstract

Communication is key in human interpersonal interaction. One critical mechanism is to communicate through speech which is mediated by the orchestration of multiple brain regions. However, knowledge of the large-scale network structure remains sparse. Here, we use a phase-based measure of functional connectivity to explore the spatiotemporal network dynamics between posterior superior temporal gyrus (pSTG) and face motor area during simple language production from subdurally implanted microelectrode arrays. One adult male undergoing invasive epilepsy monitoring was implanted with two 16-channel microelectrode arrays: one each over pSTG and face motor area. This subject was asked to produce a single word from a known list when prompted by the experimenter. Our findings show significant inter-grid correlations occurring post-speech onset. These correlations were different for each word and were found to exist predominantly in delta-band (3-4 Hz) with a peak correlation at 350 ms after onset of speech production. Such results may be consistent with auditory reafference, either through cortico-cortico circuits or mediated by autoauditory reafference.

Introduction

Speech and language are uniquely human and require the cooperation between many distinct brain regions [80]. The various functions of language have been found to be separated across various brain regions [81]. Wernicke's area (posterior aspect of the superior temporal gyrus (pSTG)) is thought to facilitate the syntactic and lexical components of language [81], [82]. Face motor cortex (inferior aspect of the primary motor cortex and associated pre-motor areas) is involved with the motor control for speech production [84].

Prior anatomical tracing and lesion studies suggest there are anatomical and functional relationships between these brain areas [82], [84], [92], [135]. These two regions assist in articulation: the transition from neural representations to motor movements. Together they are just one component of the broader language processing areas of the brain.

There are several popular recording methods to study the functional connectivity of speech in the brain. However, most of these methods are indirect measures of cortical function such as functional magnetic resonance imaging (fMRI) [34]–[38], [93] or are spatially imprecise such as electroencephalography (EEG) [39], [40]. fMRI lacks the fine millisecond temporal resolution to interrogate the temporal dynamics of speech, and EEG lacks the fine millimeter spatial resolution to interrogate the meso-scale networks that subserve speech processing.

Presently, a reasonable method for analyzing the electrophysiological functional connectivity of micro-scale networks in and between brain regions are subdurally implanted microelectrodes. Intra-cranial microelectrodes have been successful in several

human and animal research for movement and visual processing [3], [10], [20], [26], [43]–[45] . These penetrating and non-penetrating electrodes can record the brain signals at the spatial and temporal scales of neural activity [41]. These electrodes have diameters on the order of ~40 μm – 100 μm. Consequently, their listening radius are ~1 – 2 mm of cortex [41] which is on the scale of a few cortical columns [30]. Cortical columns comprise the fundamental computation units of cortical information processing. Several studies have analyzed various neuromechanisms of speech with intra-cranial microelectrodes [23], [136]–[139], but few studies to date have looked at the interrelationship between primary language areas with micro-ECoGs. The primary reason for this limitation is the difficulty in accessing patients with eloquent cortex exposure.

In patients with intractable epilepsy who require resective surgery, pre-surgical evaluation methods are used to identify the epileptogenic zone and prevent post-operative cognitive deficits. Eloquent cortex is often exposed where clinical methods and electrodes are used to determine the borders of eloquent cortex and whether eloquent cortex is affected by the epileptogenic zone. Since placement of clinical electrodes takes primacy for the purposes of patient care, it can be difficult to find room to place research electrodes on the same brain region. This is made more problematic as most clinical electrode arrays use older, larger macroelectrodes (See figure 3.1a where the research microelectrode cables run underneath the clinical macroelectrodes). Research approaches involving cortical electrodes over eloquent cortex must weigh the risk and benefits between research access and clinical access. Patient safety and clinical efficacy take precedence.

With the preponderance of evidence collected to date, we hypothesize that significant inter-region functional connections will emerge between pSTG and face motor area, time-locked with simple language production.

Methods

Subject Preparation

Data for this work was gathered from one human subject in collaboration with University of Utah, Department of Neurosurgery and under the approval of the Institutional Review Board. The subject was a patient undergoing brain mapping procedures to identify the source of medication-resistant seizures.

The patient was implanted subdurally with two 16 channel micro-ECoG grids (PMT Corporation, Chanhassen, MN). The electrodes consisted of 40 μm diameter platinum wire embedded in a thin layer of silicone with 1 mm inter-electrode spacing. (Figure 3.1c). Clinical needs and constraints drove the placement of reference and ground. One micro-ECoG grid each was placed over face motor area and the posterior aspect of superior temporal gyrus (pSTG). Reference and ground were low impedance wires placed in the epidural space.

Data Collection

All behavioral and neural data was recorded with a NeuroPort system (Blackrock Microsystems, Salt Lake City, UT). A microphone recorded the patient's speech. Neural activity and speech were recorded at 30 kHz. Data from each microelectrode were re-referenced by subtracting the common average across 16 channel blocks of electrodes,

which were located within proximity. Data for analysis were taken from -1.5 sec to 2 sec about speech onset. This data was downsampled to 1000 Hz to isolate local field potentials (LFP). A 60 Hz, 20 dB bandstop filter was applied to reduce 60 Hz noise.

The subject was recorded with a microphone and the microphone data was time aligned with the electrophysiological recording. After the experiment, the researchers manually determined the start times for each word.

Simple Language Production Task

During each block of trials the subject was given a word to speak. When instructed by an experimenter, the patient would produce the word. This would repeat between 10 and 25 trials for each word. A total of ten words were studied: yes, no, hot, cold, hungry, thirsty, more, less, hello, goodbye. Previously published work provides further detail of the experimental paradigm [23]. The subject performed the speech task with multiple sessions over several days.

Weighted Phase Lag Index

The phase lag index (PLI) is a phase-based measure of functional connectivity [140]. PLI is similar to the cross-correlation function. However, PLI removes the contribution due to volume conduction whereas cross correlation does not [140]. The PLI was modified and improved upon to create the weighted phase lag index (wPLI) [141]. This improved analysis is more robust against uncorrelated noise sources and has an increased ability to detect phase coupling.

Given a signal $x(t)$ and its Hilbert transform $\tilde{x}(t)$, the instantaneous phase $\phi(t)$ of the signal may be calculated as the phase angle of the analytic signal $z(t) = x(t) + i\tilde{x}(t)$ (Eq 3.1). Two signals are coupled if their instantaneous phase difference ($\Delta\phi(t) = \phi_2(t) - \phi_1(t)$) is asymmetrically distributed over 0 to 2π. If two signals are phase-locked at close to $\pi/2$ or $3\pi/2$ then it can be said that those two signals are coupled (Eqn 2).

$$\phi(t) = \arctan\left(\frac{\tilde{x}(t)}{x(t)}\right). \quad \text{(Eq. 3.1)} \qquad wPLI = \frac{\left|E\{|\Delta\phi(t)|\text{sign}(\Delta\phi(t))\}\right|}{E\{|\Delta\phi(t)|\}}. \quad \text{(Eq. 3.2)}$$

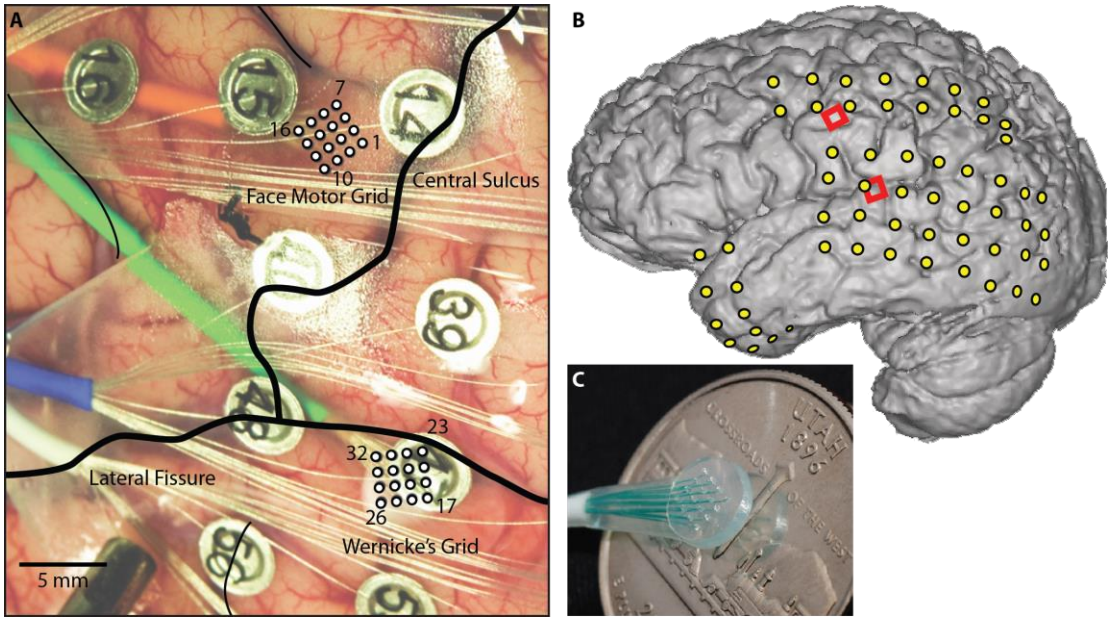

Figure 3.1. Surgical Image and Electrode Placement. A) Surgical image of the micro-ECoG electrode placement (green and orange cables) implanted beneath the macro-ECoG arrays (silver disks). Cortical landmarks have been annotated. B) MRI of patient with electrodes annotated. The micro-ECoG grids are labeled with red squares. C) Image of the micro-ECoG grids.

For this work, the wPLI was computed for 100 ms windows with 90 ms overlap for each word for each trial from -1.5 sec to +2.5 sec around speech onset for each inter-grid channel pair.

To test for significance, a set of independent and temporally uncorrelated data need to be generated to find a surrogate wPLI. A set of 500 surrogate wPLI values were computed by generating the fast Fourier transform (FFT) of the LFP data for one of the channels in the comparison. The phase information was then randomly shuffled and the inverse FFT (iFFT) was computed to create a phase-shifted LFP signal [142]. The wPLI was then computed as above.

The appearance of face motor – pSTG functional connectivity will be assessed by analyzing the wPLI values for inter-grid channel pairs (channels 1-16 (Face motor cortex) paired with channels 17-32 (pSTG)). This analysis results in a total of 256 channel pairs that were analyzed (the 16 channels of face motor cortex each paired with all 16 channels of pSTG). Significance is determined by computing the z-score between the wPLI and surrogate wPLI. A threshold value of 3 was used for this work. This process was repeated for each frequency bin of interest: delta (1, 3 Hz), theta (4, 7 Hz), alpha (8, 15 Hz), beta (16, 31 Hz), gamma (32, 79 Hz), and chi (80, 160 Hz). Analyzing 256 channel pairs across 6 frequency bands yields 1536 total comparisons.

Table 3.1

Number of trials recorded for each word and average articulation duration.

Word	Trials	Mean Duration (seconds)	Word	Trials	Mean Duration (seconds)
Yes	166	0.668	No	160	0.587
Hot	65	0.239	Cold	65	0.443
Hungry	67	0.529	Thirsty	65	0.560
Hello	69	0.536	Goodbye	65	0.621
More	65	0.481	Less	67	0.671

The number of trials that were recorded for each word, and the average length of speech, over four days of experimental recording. A total of 854 trials were recorded. Average speech length over all words is 0.575 seconds. Spoken words ranged from 0.105 seconds to 0.884 seconds.

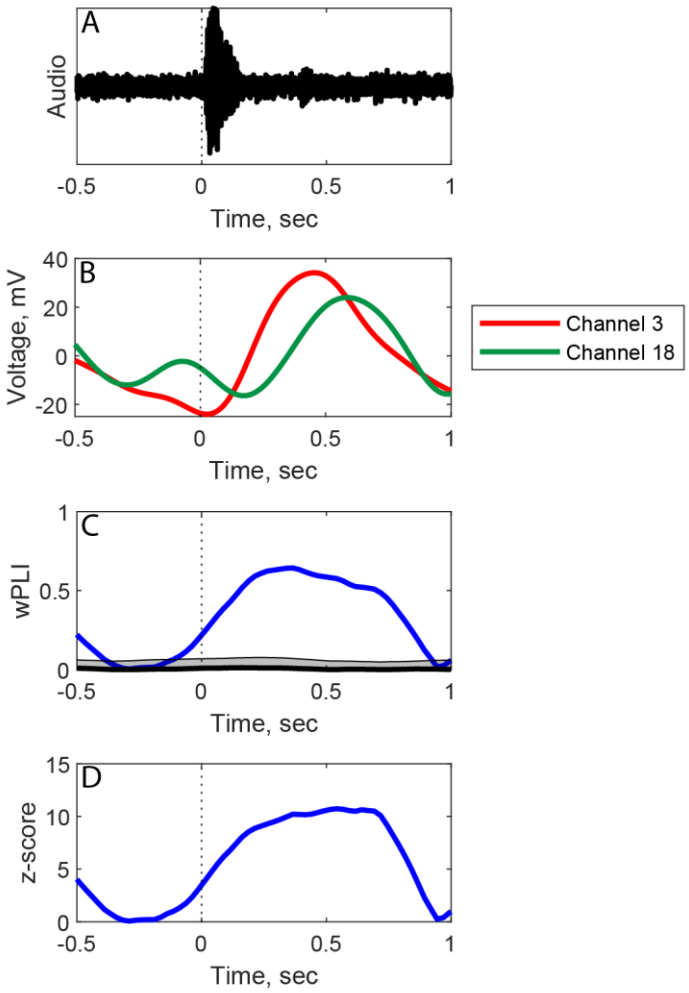

Figure 3.2. Audio, wPLI, z-score, and delta band LFP average example for the word 'hot'. A) Audio waveforms of the patient speaking the word hot. Dotted line indicated speech onset at time = 0 seconds. B) The delta band LFP average for the word 'hot' on channels 3 (face motor cortex) and 18 (pSTG). C) The computed wPLI value for the inter-grid channel pair between channels 3 and 18. The black line and grey area indicate the mean and +/- 2 standard deviation for the surrogate data. D) The computed z-scores of the wPLI value.

Results

Primary results show that inter-grid channel pairs can be coupled, time-aligned with speech onset during the simple language production task (Figure 3.2). Each analysis involved 256 inter-grid comparisons, and every word reported significantly coupled with a z-score greater than 3 (Figure 3.3, 3.7a). The active inter-grid channel pairs varied between words (Figure 3.3, 3.4, 3.5). From another perspective, there were neighboring channels would have variable participations in the inter-grid coupling for different words (Figure 3.5). Although some regularity in coupling and channel participation were observed between separate words (Figure 3.4, 3.5).

Variability in the inter-grid coupling was present between sessions, and may be due to several factors including medication, arousal, or attention, which could result in the patient varying the strength of articulation; or device-related issues such as micro-motion of the electrodes relative to the cortex due to seizure activity.

Temporal dynamics were observed for each word (Figure 3.6, 3.7a). Some words would display an increase of the number of inter-grid couplings from a pre-articulation baseline before speech onset (Figure 3.7a) with an average time of 1.5x increase from baseline at -50 ms. Baseline was calculated by averaging the 450-350 ms before speech onset (Table 3.2). The peak number of couplings occurs between 100-600 ms post-speech onset (mean 364 ms) (Figure 3.7a). The words could express between 214% and 1314% (mean 590%) increase in the number couplings post-speech onset compared with the baseline period (Figure 3.7a). These increases persisted for up to one second post-speech onset (Figure 3.7a) whereas actual speech duration ranged between 250-700 ms (Table 3.1). Simultaneously, the average strength of each coupling also increased post-speech

onset (Figure 3.8a). Although this process was highly variable between words, each word expressed a similar dynamic (Figure 3.8a).

Significant inter-grid coupling was observed for each of the frequencies tested. However, only delta-band couplings expressed trends in temporal and spatial dynamics. The other frequencies expressed baseline levels of coupling (Figure 3.7, 3.8), and under the All Words analysis category (black line) no significant inter-grid couplings were observed.

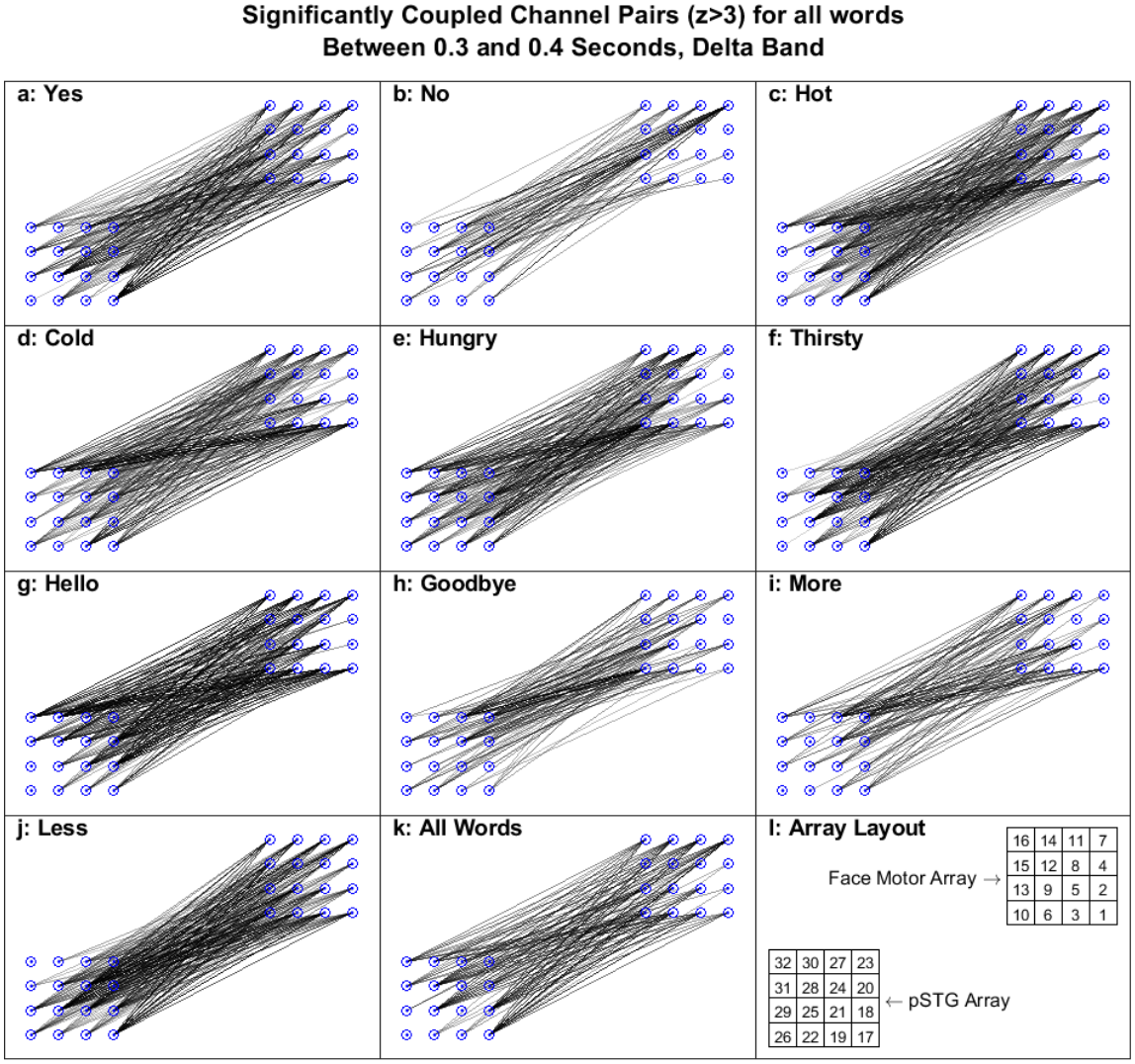

Figure 3.3. Significantly coupled inter-grid channel pairs by word, 0.3 to 0.4 seconds after speech onset. Subfigures a-j represent each of the ten words spoken during this experiment. Subfigure k shows the significant couplings when all word trials are used. Subfigure l displays the microelectrode array layout. The darker the line, the more significant the coupling.

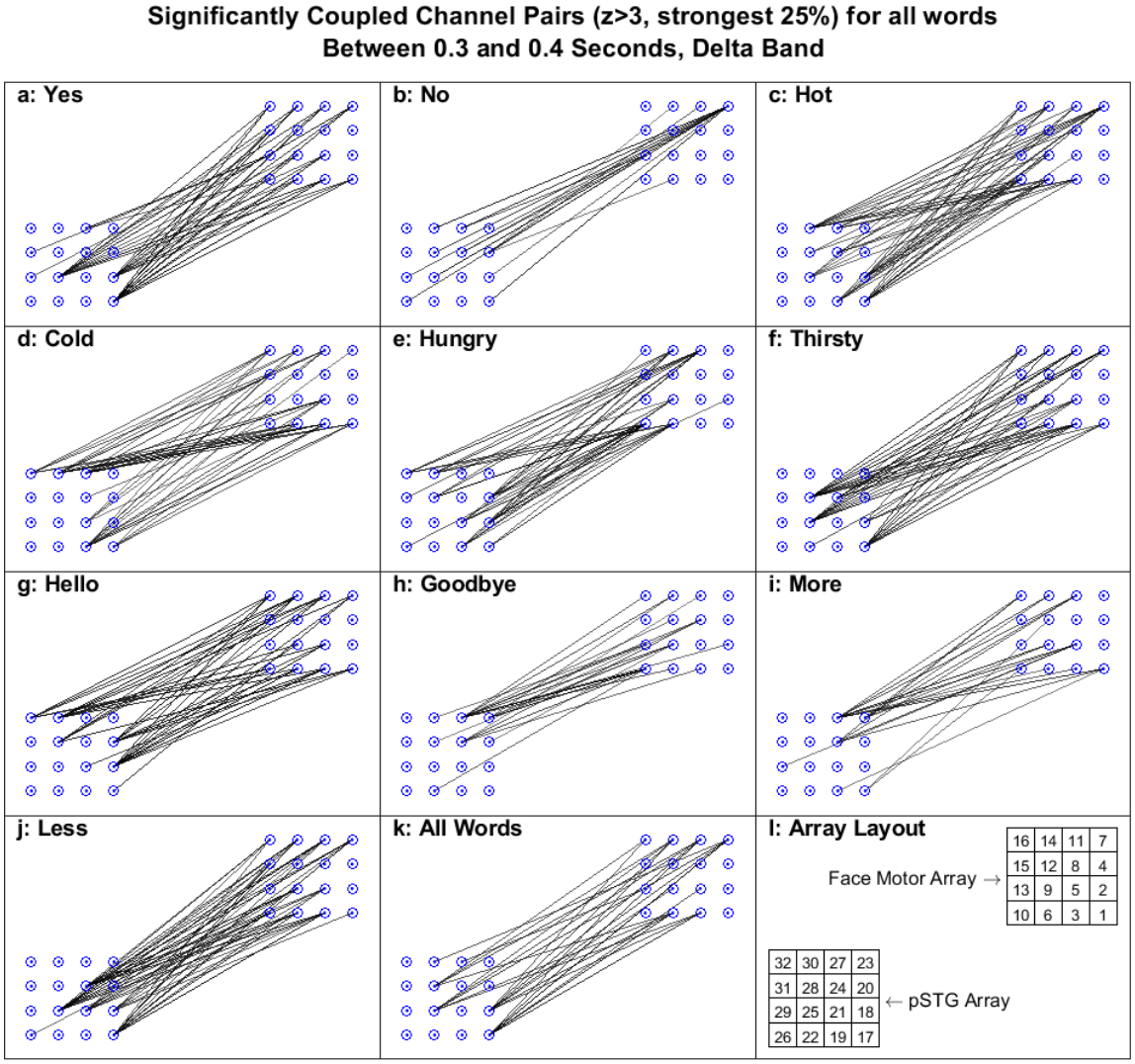

Figure 3.4. The top quartile of the significantly coupled inter-grid channel pairs by word, 0.3 to 0.4 seconds after speech onset. Subfigures a-j represent each of the ten words spoken during this experiment. Subfigure k shows the significant couplings when all word trials are used. Subfigure l displays the microelectrode array layout.

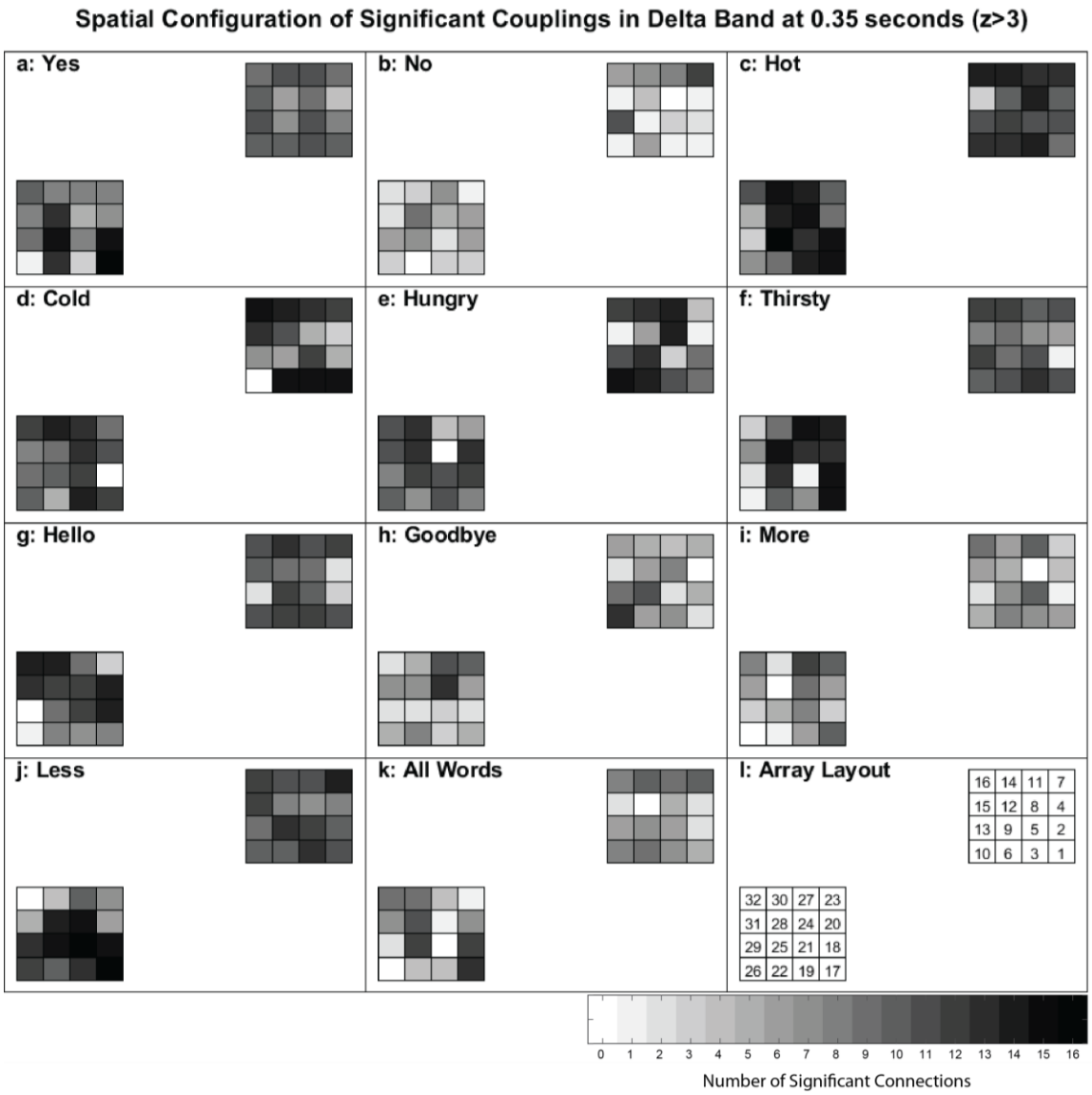

Figure 3.5. Spatial layout of inter-grid coupling channel participation. Subfigures a-k show a heatmap of the number of connections each channel was connected to with darker areas representing more connections. The values range from 0 to 16 channels.

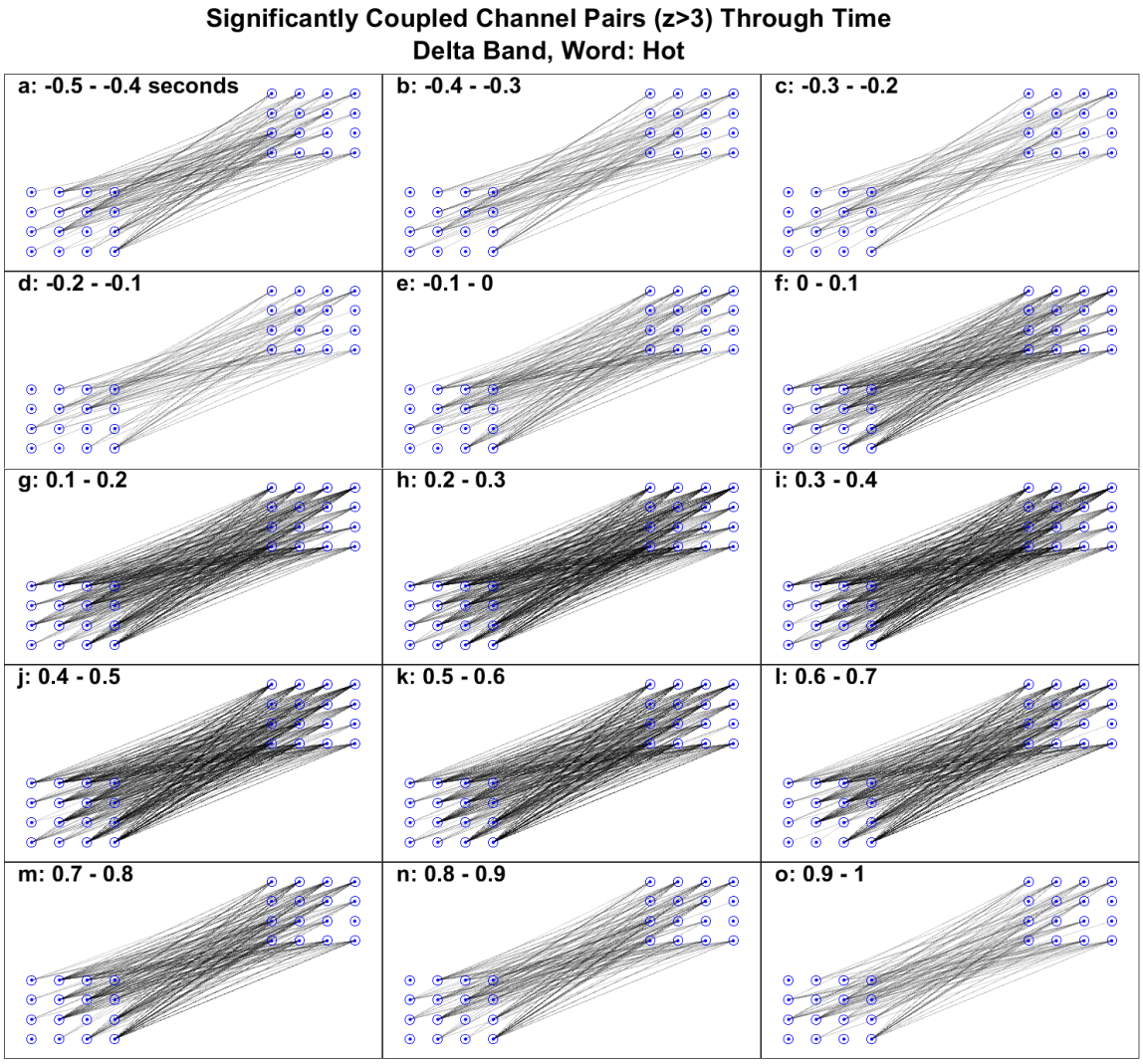

Figure 3.6. Inter-grid coupled channel pairs for the word ‘hot’ over time. Subfigures a-o represent 100 ms windows ranging from -0.5 seconds to 1 second about speech onset. Individual lines between electrode pairs represent significant coupling. The darker the line the more significant the correlation.

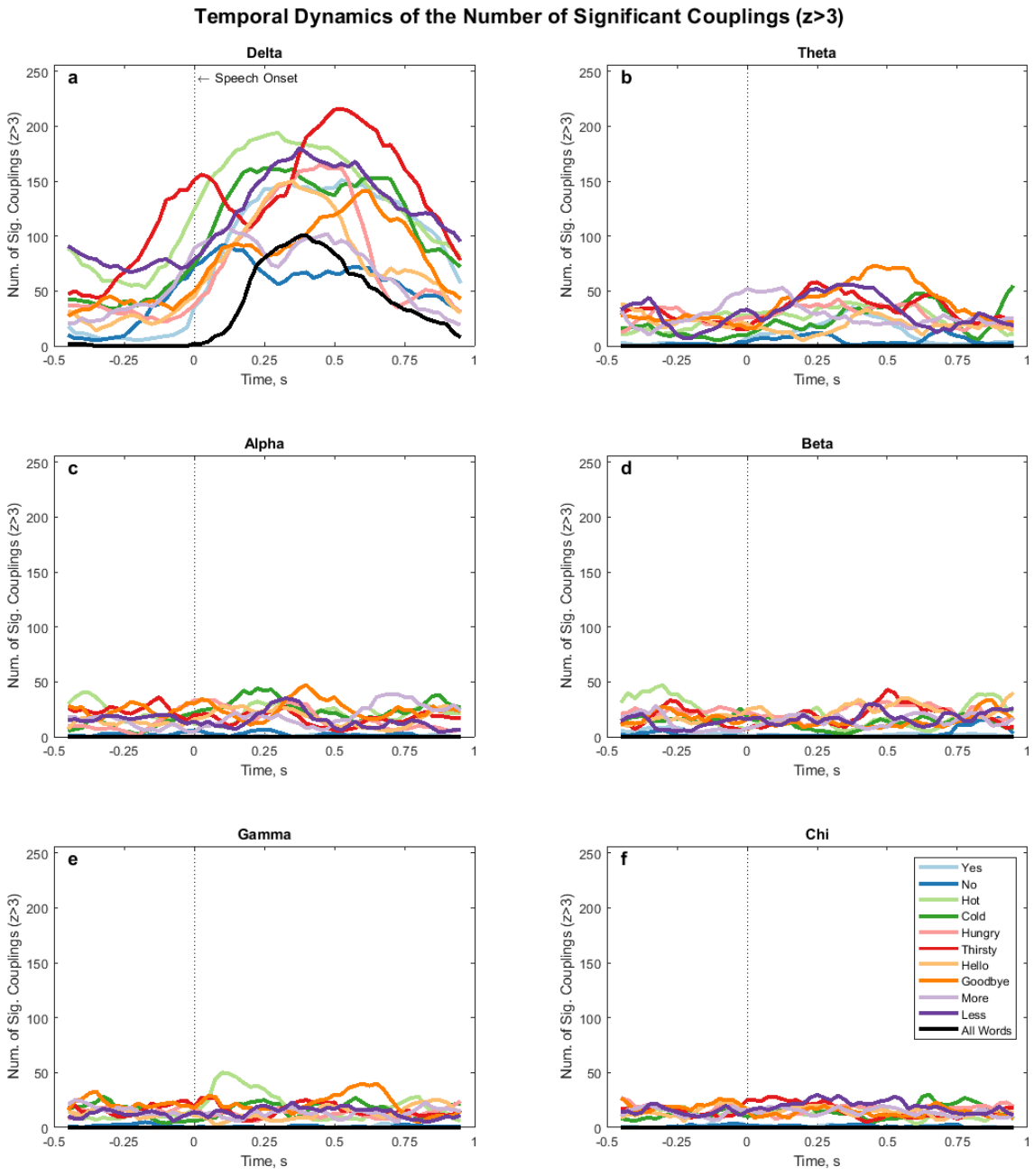

Figure 3.7. Number of significant channel pairs over time by word and frequency. The colored lines indicated the number of significantly coupled channel pairs for that word. The black line indicates the average number of significantly coupled channel when all trials were used in the computation of wPLI. Delta-band expressed the greatest number of significantly coupled inter-grid channel pairs.

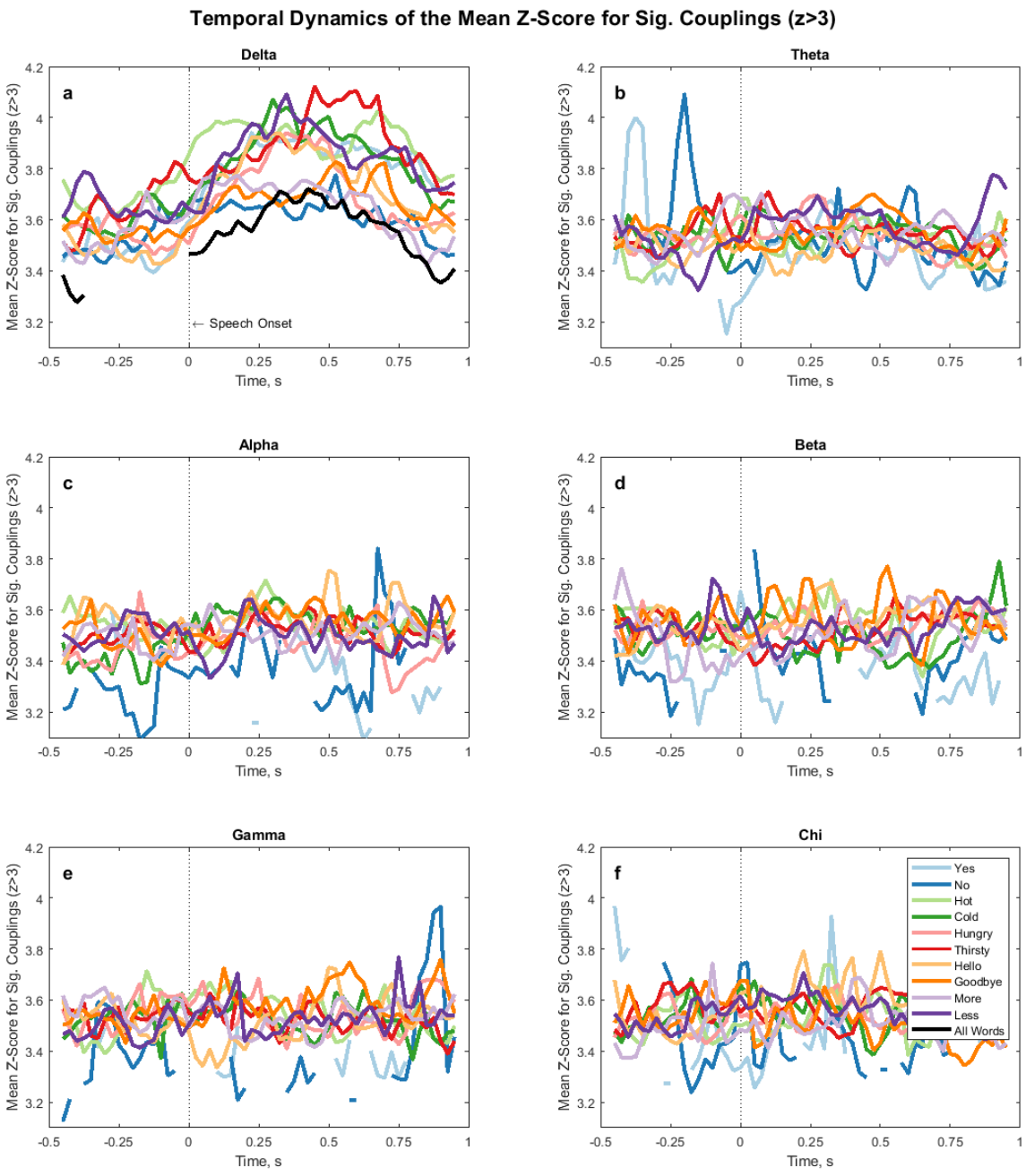

Figure 3.8. Mean z-score of significant coupling pairs by word and frequency. The colored lines indicate the mean z-score of the channels pairs which exceed $z = 3$. The black line indicates the average number of significantly coupled channel when all trials were used in the computation of wPLI. Missing sections of each line correspond to times when all z-scores dropped below 3.

Table 3.2

Time points where the number of significant couplings exceeded 1.5x baseline.

Word	Baseline Num. Sig. Couplings	Time of 1.5x increase (milliseconds)	Word	Baseline Num. Sig. Couplings	Time of 1.5x increase (milliseconds)
Yes	12.0	0	Hello	23.6	-25
No	7.0	-225	Goodbye	32.2	0
Hot	77.2	0	More	22.4	-225
Cold	40.6	-25	Less	84.0	200
Hungry	36.6	75	Average	38.2	-50
Thirsty	46.6	-225	All Words	1.4	50

The baseline number of significant couplings for each word and the time about speech onset (0 seconds) where the baseline number is exceeded by 1.5 times (Figure, 3.7). Baseline number of couplings is the average number of couplings between 450-350 ms prior to speech onset.

Discussion

Speech is a complicated process involving numerous cortical areas each responsible for a separate step of the speech production process; broadly: initiation, lexical and lemma access, phonological encoding, syllabification, and articulation [34], [87], [88], [143]–[147]. The duration between the presentation of a visual cue and a subject articulating a response can range up to 600 ms [146]. The time course of the speech production process has largely been studied with noninvasive methodologies: fMRI, electroencephalography (EEG), magnetoencephalography (MEG), and transcranial magnetic stimulation (TMS) [146], [148]–[153]. There have also been several studies using more invasive, intracranial methods [13], [154]. In this study we are contributing to

this body of work by examining the micro-scale interrelationship between pSTG and face motor area using cortical micro-ECoGs.

We examined 10 words with a phase-based analysis to find micro-scale functional connections between face motor area and pSTG. The existence of such a network between face motor and pSTG areas can only be mediated by cortico-cortico connections through the brain. For the 10 words studied (excluding the All Words case), baseline number of significant delta-band couplings increased by 1.5 times prior to speech onset with an average of -50 ms delay (Figure 3.7). For half of the words (no, hot, thirsty, more, hello) the coupling between pSTG and face motor area increased by 1.5 times at 200 ms before speech onset (Figure 3.7a, Table 3.2). This finding is in line with previous MEG and TMS studies on the temporal difference between peak activation of pSTG and Broca's area (200-400ms) [148]–[153]. The other words that were not found to have a large pre-articulation increase in inter-region coupling may be more connected in parts of cortex that were outside the listening radius of the micro-ECoG arrays. We have also observed that amount of inter-region delta-band coupling peaked in the 250-400 ms range after speech onset. This period of maximal delta-band coupling falls into the range where disfluencies in delayed auditory feedback (DAF) tasks peak; around 200-250 ms delay [155]–[157]. It has been shown that DAF tasks can, paradoxically, improve the symptoms of patients with speech disfluencies [158]–[160], perhaps by regularizing or resetting an internal time-keeping signal [157], [161], [162]. The inter-region delta-band coupling was observed to slowly return to baseline after articulation, though the tailing affect is most likely due to the variance in articulation length between trails of the same word.

Time evolving dynamic interactions were found to occur only in delta-band (0.1-3 Hz). At higher frequencies the All Words category found no significant inter-region coupling pre-articulation, during articulation, or post-articulation. Strongly suggesting that these higher frequency bands are not phase-coupled. Delta-band does not oscillate fast enough to support all the phonologic information necessary to support speech production. Instead, it is likely that the wPLI analysis is ill-suited to extract high frequency features of neural communication. Additional analysis may reveal that high frequency functional connectivity metrics are phase-amplitude coupled to delta-band phase coupling, rather than time-locked to speech onset. Such a finding would provide insight into the interplay between the parallel neural functional connectivity mechanisms that coordinate speech.

The All Words line (black) in delta-band (Figure 3.7a) may represent a default-mode of the inter-region coupling, where the delta-band signal corresponds to some common need for inter-region coherence during articulation. Together, the pre-articulation increase from baseline coupling, peak coupling during the vulnerable period for DAF, and the presence of coupling post-articulation may provide evidence that the delta-band coupling signal is related to the coordination and facilitation of speech production. The presence of a delta-band inter-region coupling signal after speech onset (presumably after the motor programs have been crafted) may be a sign of auditory reafference or an efference copy of the expected articulation. Future studies with focus on overt/covert speech or interrogating the effects of DAF_{ON} and DAF_{OFF} cases may be able to yield more insight on the purpose of the delta-band inter-region in the post-speech onset regime.

When only the top quartile of inter-grid coupling with the largest z-score were displayed, a potential structure of connectivity emerges for some of the words (Figure 3.7cdefg). Such a consistent, stable, structure of connectivity may suggest that there is a common geometry of this cortico-cortico network involved in the coordination and facilitation of cortical processing of speech features. A further study of this network geometry may reveal causal directions of information exchange that subserve the coordination between brain regions during simple language production.

We have validated that microelectrodes can record interesting and potentially useful cortical-cortical electrophysiological functional connections between language areas. Microelectrodes appear to be well matched to this use case due to the observed spatial discreetness of detected functional connections and the relatively limited spatial extent of face motor cortex and Wernicke's area. Microelectrode arrays with more electrodes could potentially cover the entire expanse of these studied language areas.

CHAPTER 4

CONCLUSION

Complex network dynamics mediate information processing in the brain between anatomically local (intra-cortical areas) and distant (between distinct cortical and subcortical areas) regions. Electrophysiological functional connectivity describes the temporal correlations between neurophysiological events (LFP / AP) that are spatially remote, without regard to anatomical connectivity that may or may not be apparent between them. At present, intra-cranial microelectrodes offer a path to study the network dynamics of cognition or disease at the millimeter and millisecond scales, the same spatial and temporal scales as cortical columns, the foundational unit of neural computation. The work shown in this document display the feasibility of microelectrodes to study electrophysiological functional connectivity. A key consideration for future work is to precisely place and localize the placement of microelectrodes to ensure the brain regions being studied are relevant to the hypothesis being tested.

Micro-Scale Cortico-Basal Ganglia Functional Connectivity in Parkinson's Disease

Parkinson's disease is a degenerative neurological disorder afflicting the motor system, associated with impairments such as bradykinesia, tremor, and impaired balance. The exact mechanisms causing these symptoms are unknown [67], but their progression is associated with the loss of dopaminergic cells in the SNR. This pathological imbalance of neurotransmitters could interrupt the selection and inhibition of voluntary movements resulting in the movement impairments associated with Parkinson's disease [67], [69].

To study and probe the effects of Parkinson's disease on the cortico-basal ganglia loop this study used subdurally placed micro-ECoG arrays over premotor cortex and penetrating FHC microelectrodes in basal ganglia. These devices were chosen because they allow us to investigate the electrophysiological functional connectivity between basal ganglia and cortex at the same spatial and temporal scales of neural computation.

Significant cortico-basal ganglia functional connections were observed in patients undergoing DBS implantation to treat Parkinson's disease in 83 of 127 isolated neurons. These functional connections were observed in each of theta, alpha, beta, gamma, chi, and AP frequency bands. Micro-scale networks were observed to be highly granular in space, with neighboring electrodes of the micro-ECoG, just 2 mm apart, expressing different significance. 12 neurons expressed functional connections, in multiple frequency bands, to different regions of the cortical micro-ECoG, suggesting that these neurons are embedded in multiple, parallel networks. By an order of magnitude, the AP-band expressed the most connectivity and demonstrated a consistent delay across patients at +50 ms from the AP time suggesting the presence of neuron-neuron population cortico-basal ganglia coupling.

As all recordings studied were taken from anesthetized patients, our findings may reflect the default mode network interactions, rather than cortical-subcortical interactions responsible for the presentation of symptoms. As the subjects have been diagnosed with Parkinson's for many years our observations may reflect compensatory changes in the cortical-subcortical circuitry or long-term effects of chronic levodopa therapy [134], instead of the underlying disorder.

Future work can address these limitations by designing experiments with awake and behaving patients in mind. As an example, studying motor or cognitive motor tasks (rigidity and festination [163], cognitive effort discounting [164]) under different conditions (on/off meds, on/off therapeutic stimulation). Of course, there would not be enough time to fully explore the combinations between tasks and conditions intraoperatively, so a postoperative externalization approach would be recommended [165].

Reciprocal Functional Connectivity Between pSTG and Face Motor Cortex During Simple Language Production

Speech is a complicated process involving numerous cortical areas each responsible for a separate step of the speech production process; broadly: initiation, lexical and lemma access, phonological encoding, syllabification, and articulation [34], [87], [88], [143]–[147]. The duration between the presentation of a visual cue and a subject articulating a response can range up to 600 ms [146]. The time course of the speech production process has largely been studied with noninvasive methodologies: fMRI, EEG, MEG, and TMS [146], [148]–[153]. In this study we are contributing to this body of work by examining the micro-scale interrelationship between pSTG and face motor area using cortical micro-ECoGs.

Our main finding was the presence of reciprocal functional connectivity between pSTG and face motor area in delta-band. For half of the words, this coupling initiated prior to speech onset with a delay of -200 ms which matches the temporal delay found in prior MEG studies [148]–[153]. This coupling signal remained high throughout

articulation before finally returning to baseline 200 ms after speech termination. Of particular note relating to the micro-scale electrodes, we observed unique network geometries that evolved smoothly over time. Since delta-band is not fast enough to contain all the information necessary for speech articulation, it may be that the delta-band signal facilitates or coordinates the exchange of information or interoperation between pSTG and face motor area. The persistence and reciprocal nature of the functional connectivity may also be related to auditory reafference and sensory attenuation through an efference copy of the expected articulation.

We were only able to detect phase coupling in delta-band, implying that the wPLI algorithm may be ill-suited to the analysis of higher frequency phase coupling. Additional analysis may reveal that high frequency functional connectivity metrics are phase-amplitude coupled to delta-band phase coupling, rather than time-locked to speech onset. In addition to additional analysis methods, future studies may also explore the difference between overt and covert speech, homophones, and delayed auditory feedback.

REFERENCES

[1] U. Mitzdorf, “Current source-density method and application in cat cerebral cortex: investigation of evoked potentials and EEG phenomena,” *Physiol. Rev.*, vol. 65, no. 1, pp. 37–100, Jan. 1985, doi: 10.1152/physrev.1985.65.1.37.

[2] U. Mitzdorf, “Properties of the evoked potential generators: current source-density analysis of visually evoked potentials in the cat cortex,” *Int. J. Neurosci.*, vol. 33, no. 1–2, pp. 33–59, Mar. 1987, doi: 10.3109/00207458708985928.

[3] A. K. Engel, P. König, C. M. Gray, and W. Singer, “Stimulus-Dependent Neuronal Oscillations in Cat Visual Cortex: Inter-Columnar Interaction as Determined by Cross-Correlation Analysis,” *Eur. J. Neurosci.*, vol. 2, no. 7, pp. 588–606, 1990, doi: 10.1111/j.1460-9568.1990.tb00449.x.

[4] T. H. Bullock, “Signals and signs in the nervous system: The dynamic anatomy of electrical activity is probably information-rich,” *Proc. Natl. Acad. Sci.*, vol. 94, no. 1, pp. 1–6, Jan. 1997, doi: 10.1073/pnas.94.1.1.

[5] W. J. Freeman and J. M. Barrie, “Analysis of spatial patterns of phase in neocortical gamma EEGs in rabbit,” *J. Neurophysiol.*, vol. 84, no. 3, pp. 1266–1278, Sep. 2000, doi: 10.1152/jn.2000.84.3.1266.

[6] G. Buzsáki, C. A. Anastassiou, and C. Koch, “The origin of extracellular fields and currents--EEG, ECoG, LFP and spikes,” *Nat. Rev. Neurosci.*, vol. 13, no. 6, pp. 407–420, May 2012, doi: 10.1038/nrn3241.

[7] C. Mehring *et al.*, “Comparing information about arm movement direction in single channels of local and epicortical field potentials from monkey and human motor cortex,” *J. Physiol. Paris*, vol. 98, no. 4–6, pp. 498–506, Nov. 2004, doi: 10.1016/j.jphysparis.2005.09.016.

[8] S. Ray, N. E. Crone, E. Niebur, P. J. Franaszczuk, and S. S. Hsiao, “Neural correlates of high-gamma oscillations (60-200 Hz) in macaque local field potentials and their potential implications in electrocorticography,” *J. Neurosci. Off. J. Soc. Neurosci.*, vol. 28, no. 45, pp. 11526–11536, Nov. 2008, doi: 10.1523/JNEUROSCI.2848-08.2008.

[9] V. B. Mountcastle, “Modality and topographic properties of single neurons of cat’s somatic sensory cortex,” *J. Neurophysiol.*, vol. 20, no. 4, pp. 408–434, Jul. 1957, doi: 10.1152/jn.1957.20.4.408.

[10] W. Singer and C. M. Gray, “Visual feature integration and the temporal correlation hypothesis,” *Annu. Rev. Neurosci.*, vol. 18, pp. 555–586, 1995, doi: 10.1146/annurev.ne.18.030195.003011.

[11] A. P. Georgopoulos, M. Taira, and A. Lukashin, “Cognitive neurophysiology of the motor cortex,” *Science*, vol. 260, no. 5104, pp. 47–52, Apr. 1993, doi: 10.1126/science.8465199.

[12] B. Amirikian and A. P. Georgopoulos, “Modular organization of directionally tuned cells in the motor cortex: Is there a short-range order?,” *Proc. Natl. Acad. Sci. U. S. A.*, vol. 100, no. 21, pp. 12474–12479, Oct. 2003, doi: 10.1073/pnas.2037719100.

[13] A. Flinker, E. F. Chang, N. M. Barbaro, M. S. Berger, and R. T. Knight, “Sub-centimeter language organization in the human temporal lobe,” *Brain Lang.*, vol. 117, no. 3, pp. 103–109, Jun. 2011, doi: 10.1016/j.bandl.2010.09.009.

[14] J. Liu and W. T. Newsome, “Local field potential in cortical area MT: stimulus tuning and behavioral correlations,” *J. Neurosci. Off. J. Soc. Neurosci.*, vol. 26, no. 30, pp. 7779–7790, Jul. 2006, doi: 10.1523/JNEUROSCI.5052-05.2006.

[15] S. Łęski, H. Lindén, T. Tetzlaff, K. H. Pettersen, and G. T. Einevoll, “Frequency dependence of signal power and spatial reach of the local field potential,” *PLoS Comput. Biol.*, vol. 9, no. 7, p. e1003137, 2013, doi: 10.1371/journal.pcbi.1003137.

[16] S. Katzner, I. Nauhaus, A. Benucci, V. Bonin, D. L. Ringach, and M. Carandini, “Local origin of field potentials in visual cortex,” *Neuron*, vol. 61, no. 1, pp. 35–41, Jan. 2009, doi: 10.1016/j.neuron.2008.11.016.

[17] D. Xing, C.-I. Yeh, and R. M. Shapley, “Spatial spread of the local field potential and its laminar variation in visual cortex,” *J. Neurosci. Off. J. Soc. Neurosci.*, vol. 29, no. 37, pp. 11540–11549, Sep. 2009, doi: 10.1523/JNEUROSCI.2573-09.2009.

[18] G. Kreiman, C. P. Hung, A. Kraskov, R. Q. Quiroga, T. Poggio, and J. J. DiCarlo, “Object selectivity of local field potentials and spikes in the macaque inferior temporal cortex,” *Neuron*, vol. 49, no. 3, pp. 433–445, Feb. 2006, doi: 10.1016/j.neuron.2005.12.019.

[19] P. Berens, G. A. Keliris, A. S. Ecker, N. K. Logothetis, and A. S. Tolias, “Comparing the Feature Selectivity of the Gamma-Band of the Local Field Potential and the Underlying Spiking Activity in Primate Visual Cortex,” *Front. Syst. Neurosci.*, vol. 2, Jun. 2008, doi: 10.3389/neuro.06.002.2008.

[20] X. Jia, M. A. Smith, and A. Kohn, “Stimulus Selectivity and Spatial Coherence of Gamma Components of the Local Field Potential,” *J. Neurosci.*, vol. 31, no. 25, pp. 9390–9403, Jun. 2011, doi: 10.1523/JNEUROSCI.0645-11.2011.

[21] M. Seyedhosseini *et al.*, “Informative features of local field potential signals in primary visual cortex during natural image stimulation,” *J. Neurophysiol.*, vol. 113, no. 5, pp. 1520–1532, Mar. 2015, doi: 10.1152/jn.00278.2014.

[22] W. Wang *et al.*, “Human motor cortical activity recorded with Micro-ECoG electrodes, during individual finger movements,” *Conf. Proc. Annu. Int. Conf. IEEE Eng. Med. Biol. Soc. IEEE Eng. Med. Biol. Soc. Annu. Conf.*, vol. 2009, pp. 586–589, 2009, doi: 10.1109/IEMBS.2009.5333704.

[23] S. Kellis, K. Miller, K. Thomson, R. Brown, P. House, and B. Greger, “Decoding spoken words using local field potentials recorded from the cortical surface,” *J. Neural Eng.*, vol. 7, no. 5, p. 056007, Oct. 2010, doi: 10.1088/1741-2560/7/5/056007.

[24] H. Panagiotides, W. J. Freeman, M. D. Holmes, and D. Pantazis, “Behavioral states may be associated with distinct spatial patterns in electrocorticogram,” *Cogn. Neurodyn.*, vol. 5, no. 1, pp. 55–66, Mar. 2011, doi: 10.1007/s11571-010-9139-4.

[25] B. Pesaran, J. S. Pezaris, M. Sahani, P. P. Mitra, and R. A. Andersen, “Temporal structure in neuronal activity during working memory in macaque parietal cortex,” *Nat. Neurosci.*, vol. 5, no. 8, pp. 805–811, Aug. 2002, doi: 10.1038/nn890.

[26] P. Fries, “Neuronal gamma-band synchronization as a fundamental process in cortical computation,” *Annu. Rev. Neurosci.*, vol. 32, pp. 209–224, 2009, doi: 10.1146/annurev.neuro.051508.135603.

[27] M. Aghagolzadeh, L. R. Hochberg, S. S. Cash, and W. Truccolo, “Predicting Seizures from Local Field Potentials Recorded via Intracortical Microelectrode Arrays,” *Conf. Proc. Annu. Int. Conf. IEEE Eng. Med. Biol. Soc. IEEE Eng. Med. Biol. Soc. Annu. Conf.*, vol. 2016, pp. 6353–6356, Aug. 2016, doi: 10.1109/EMBC.2016.7592181.

[28] J. V. Rosenfeld and Y. T. Wong, “Neurobionics and the brain-computer interface: current applications and future horizons,” *Med. J. Aust.*, vol. 206, no. 8, pp. 363–368, May 2017, doi: 10.5694/mja16.01011.

[29] W. Penfield and H. Jasper, *Epilepsy and the functional anatomy of the human brain*. Oxford, England: Little, Brown & Co., 1954.

[30] V. B. Mountcastle, “The columnar organization of the neocortex,” *Brain J. Neurol.*, vol. 120 (Pt 4), pp. 701–722, Apr. 1997, doi: 10.1093/brain/120.4.701.

[31] S. Zhang, A. T. Connolly, L. R. Madden, J. L. Vitek, and M. D. Johnson, “High-resolution local field potentials measured with deep brain stimulation arrays,” *J. Neural Eng.*, vol. 15, no. 4, p. 046019, 2018, doi: 10.1088/1741-2552/aabdf5.

[32] A. Ramirez-Zamora *et al.*, “Evolving Applications, Technological Challenges and Future Opportunities in Neuromodulation: Proceedings of the Fifth Annual Deep Brain Stimulation Think Tank,” *Front. Neurosci.*, vol. 11, Jan. 2018, doi: 10.3389/fnins.2017.00734.

[33] P. J. Basser, J. Mattiello, and D. LeBihan, “MR diffusion tensor spectroscopy and imaging.,” *Biophys. J.*, vol. 66, no. 1, pp. 259–267, Jan. 1994.

[34] G. Hickok and D. Poeppel, “The cortical organization of speech processing,” *Nat. Rev. Neurosci.*, vol. 8, no. 5, pp. 393–402, May 2007, doi: 10.1038/nrn2113.

[35] D. Poeppel, “The neuroanatomic and neurophysiological infrastructure for speech and language,” *Curr. Opin. Neurobiol.*, vol. 28, pp. 142–149, Oct. 2014, doi: 10.1016/j.conb.2014.07.005.

[36] F. Pulvermüller and L. Fadiga, “Active perception: sensorimotor circuits as a cortical basis for language,” *Nat. Rev. Neurosci.*, vol. 11, no. 5, pp. 351–360, May 2010, doi: 10.1038/nrn2811.

[37] K. Simonyan and B. Horwitz, “Laryngeal Motor Cortex and Control of Speech in Humans,” *Neurosci. Rev. J. Bringing Neurobiol. Neurol. Psychiatry*, vol. 17, no. 2, pp. 197–208, Apr. 2011, doi: 10.1177/1073858410386727.

[38] L. J. Silbert, C. J. Honey, E. Simony, D. Poeppel, and U. Hasson, “Coupled neural systems underlie the production and comprehension of naturalistic narrative speech,” *Proc. Natl. Acad. Sci. U. S. A.*, vol. 111, no. 43, pp. E4687-4696, Oct. 2014, doi: 10.1073/pnas.1323812111.

[39] F. Panov *et al.*, “Intraoperative electrocorticography for physiological research in movement disorders: principles and experience in 200 cases,” *J. Neurosurg.*, vol. 126, no. 1, pp. 122–131, Jan. 2017, doi: 10.3171/2015.11.JNS151341.

[40] G. C. O’Neill, P. Tewarie, D. Vidaurre, L. Liuzzi, M. W. Woolrich, and M. J. Brookes, “Dynamics of large-scale electrophysiological networks: A technical review,” *NeuroImage*, vol. 180, no. Pt B, pp. 559–576, 15 2018, doi: 10.1016/j.neuroimage.2017.10.003.

[41] S. Kellis *et al.*, “Multi-scale analysis of neural activity in humans: Implications for micro-scale electrocorticography,” *Clin. Neurophysiol. Off. J. Int. Fed. Clin. Neurophysiol.*, vol. 127, no. 1, pp. 591–601, Jan. 2016, doi: 10.1016/j.clinph.2015.06.002.

[42] K. J. Miller, L. B. Sorensen, J. G. Ojemann, and M. den Nijs, “Power-law scaling in the brain surface electric potential,” *PLoS Comput. Biol.*, vol. 5, no. 12, p. e1000609, Dec. 2009, doi: 10.1371/journal.pcbi.1000609.

[43] C. von der Malsburg, “Binding in models of perception and brain function,” *Curr. Opin. Neurobiol.*, vol. 5, no. 4, pp. 520–526, Aug. 1995, doi: 10.1016/0959-4388(95)80014-x.

[44] G. Buzsáki and A. Draguhn, “Neuronal oscillations in cortical networks,” *Science*, vol. 304, no. 5679, pp. 1926–1929, Jun. 2004, doi: 10.1126/science.1099745.

[45] I. Ayzenshtat *et al.*, “Precise Spatiotemporal Patterns among Visual Cortical Areas and Their Relation to Visual Stimulus Processing,” *J. Neurosci.*, vol. 30, no. 33, pp. 11232–11245, Aug. 2010, doi: 10.1523/JNEUROSCI.5177-09.2010.

[46] R. L. Albin, A. B. Young, and J. B. Penney, “The functional anatomy of basal ganglia disorders,” *Trends Neurosci.*, vol. 12, no. 10, pp. 366–375, Oct. 1989, doi: 10.1016/0166-2236(89)90074-x.

[47] A. R. Crossman, “Primate models of dyskinesia: the experimental approach to the study of basal ganglia-related involuntary movement disorders,” *Neuroscience*, vol. 21, no. 1, pp. 1–40, Apr. 1987, doi: 10.1016/0306-4522(87)90322-8.

[48] M. R. DeLong, “Primate models of movement disorders of basal ganglia origin,” *Trends Neurosci.*, vol. 13, no. 7, pp. 281–285, Jul. 1990, doi: 10.1016/0166-2236(90)90110-v.

[49] J. A. Obeso, M. C. Rodriguez, and M. R. DeLong, “Basal ganglia pathophysiology. A critical review,” *Adv. Neurol.*, vol. 74, pp. 3–18, 1997.

[50] J. A. Obeso *et al.*, “Pathophysiology of the basal ganglia in Parkinson’s disease,” *Trends Neurosci.*, vol. 23, no. 10 Suppl, pp. S8-19, Oct. 2000, doi: 10.1016/s1471-1931(00)00028-8.

[51] R. Levy *et al.*, “Re-evaluation of the functional anatomy of the basal ganglia in normal and Parkinsonian states,” *Neuroscience*, vol. 76, no. 2, pp. 335–343, Jan. 1997, doi: 10.1016/s0306-4522(96)00409-5.

[52] J. A. Obeso, M. C. Rodriguez-Oroz, M. Rodriguez, and M. R. DeLong, “Current problems in understanding the basal ganglia model for Parkinson’s disease and levodopa-induced dyskinesias,” *Ann. Neurol.*, vol. 47, pp. 22–32, 2000.

[53] M. Takada, H. Tokuno, A. Nambu, and M. Inase, “Corticostriatal input zones from the supplementary motor area overlap those from the contra- rather than ipsilateral primary motor cortex,” *Brain Res.*, vol. 791, no. 1–2, pp. 335–340, Apr. 1998, doi: 10.1016/s0006-8993(98)00198-x.

[54] J. Guridi *et al.*, “Targeting the basal ganglia for deep brain stimulation in Parkinson’s disease,” *Neurology*, vol. 55, no. 12 Suppl 6, pp. S21-28, 2000.

[55] M. C. Rodriguez-Oroz *et al.*, “The subthalamic nucleus in Parkinson’s disease: somatotopic organization and physiological characteristics,” *Brain J. Neurol.*, vol. 124, no. Pt 9, pp. 1777–1790, Sep. 2001, doi: 10.1093/brain/124.9.1777.

[56] P. V. Theodosopoulos, W. J. Marks, C. Christine, and P. A. Starr, “Locations of movement-related cells in the human subthalamic nucleus in Parkinson’s disease,” *Mov. Disord. Off. J. Mov. Disord. Soc.*, vol. 18, no. 7, pp. 791–798, Jul. 2003, doi: 10.1002/mds.10446.

[57] F. A. Middleton and P. L. Strick, “Basal ganglia and cerebellar loops: motor and cognitive circuits,” *Brain Res. Brain Res. Rev.*, vol. 31, no. 2–3, pp. 236–250, Mar. 2000, doi: 10.1016/s0165-0173(99)00040-5.

[58] G. E. Alexander and M. D. Crutcher, “Functional architecture of basal ganglia circuits: neural substrates of parallel processing,” *Trends Neurosci.*, vol. 13, no. 7, pp. 266–271, Jul. 1990, doi: 10.1016/0166-2236(90)90107-l.

[59] G. E. Alexander, M. D. Crutcher, and M. R. DeLong, “Basal ganglia-thalamocortical circuits: parallel substrates for motor, oculomotor, ‘prefrontal’ and ‘limbic’ functions,” *Prog. Brain Res.*, vol. 85, pp. 119–146, 1990.

[60] G. E. Alexander, M. R. DeLong, and P. L. Strick, “Parallel Organization of Functionally Segregated Circuits Linking Basal Ganglia and Cortex,” *Annu. Rev. Neurosci.*, vol. 9, no. 1, pp. 357–381, 1986, doi: 10.1146/annurev.ne.09.030186.002041.

[61] F. A. Middleton and P. L. Strick, “Anatomical evidence for cerebellar and basal ganglia involvement in higher cognitive function,” *Science*, vol. 266, no. 5184, pp. 458–461, Oct. 1994, doi: 10.1126/science.7939688.

[62] F. A. Middleton and P. L. Strick, “Basal-ganglia ‘projections’ to the prefrontal cortex of the primate,” *Cereb. Cortex N. Y. N 1991*, vol. 12, no. 9, pp. 926–935, Sep. 2002, doi: 10.1093/cercor/12.9.926.

[63] A. Nambu, H. Tokuno, and M. Takada, “Functional significance of the cortico-subthalamo-pallidal ‘hyperdirect’ pathway,” *Neurosci. Res.*, vol. 43, no. 2, pp. 111–117, Jun. 2002, doi: 10.1016/s0168-0102(02)00027-5.

[64] K. H. Monakow, K. Akert, and H. Künzle, “Projections of the precentral motor cortex and other cortical areas of the frontal lobe to the subthalamic nucleus in the monkey,” *Exp. Brain Res.*, vol. 33, no. 3–4, pp. 395–403, Nov. 1978, doi: 10.1007/bf00235561.

[65] M. Inase, H. Tokuno, A. Nambu, T. Akazawa, and M. Takada, “Corticostriatal and corticosubthalamic input zones from the presupplementary motor area in the macaque monkey: comparison with the input zones from the supplementary motor area,” *Brain Res.*, vol. 833, no. 2, pp. 191–201, Jul. 1999, doi: 10.1016/s0006-8993(99)01531-0.

[66] M. Takada *et al.*, “Organization of inputs from cingulate motor areas to basal ganglia in macaque monkey,” *Eur. J. Neurosci.*, vol. 14, no. 10, pp. 1633–1650, Nov. 2001, doi: 10.1046/j.0953-816x.2001.01789.x.

[67] J. W. Mink, “The Basal Ganglia and involuntary movements: impaired inhibition of competing motor patterns,” *Arch. Neurol.*, vol. 60, no. 10, pp. 1365–1368, Oct. 2003, doi: 10.1001/archneur.60.10.1365.

[68] J. L. Lanciego, N. Luquin, and J. A. Obeso, “Functional Neuroanatomy of the Basal Ganglia,” *Cold Spring Harb. Perspect. Med.*, vol. 2, no. 12, Dec. 2012, doi: 10.1101/cshperspect.a009621.

[69] J. W. Mink, “The basal ganglia: focused selection and inhibition of competing motor programs,” *Prog. Neurobiol.*, vol. 50, no. 4, pp. 381–425, Nov. 1996, doi: 10.1016/s0301-0082(96)00042-1.

[70] P. Brown, “Abnormal oscillatory synchronisation in the motor system leads to impaired movement,” *Curr. Opin. Neurobiol.*, vol. 17, no. 6, pp. 656–664, Dec. 2007, doi: 10.1016/j.conb.2007.12.001.

[71] P. Khanna and J. M. Carmena, “Neural oscillations: beta band activity across motor networks,” *Curr. Opin. Neurobiol.*, vol. 32, pp. 60–67, Jun. 2015, doi: 10.1016/j.conb.2014.11.010.

[72] E. Lalo *et al.*, “Patterns of bidirectional communication between cortex and basal ganglia during movement in patients with Parkinson disease,” *J. Neurosci. Off. J. Soc. Neurosci.*, vol. 28, no. 12, pp. 3008–3016, Mar. 2008, doi: 10.1523/JNEUROSCI.5295-07.2008.

[73] J. López-Azcárate *et al.*, “Coupling between beta and high-frequency activity in the human subthalamic nucleus may be a pathophysiological mechanism in Parkinson’s disease,” *J. Neurosci. Off. J. Soc. Neurosci.*, vol. 30, no. 19, pp. 6667–6677, May 2010, doi: 10.1523/JNEUROSCI.5459-09.2010.

[74] C. de Hemptinne *et al.*, “Exaggerated phase–amplitude coupling in the primary motor cortex in Parkinson disease,” *Proc. Natl. Acad. Sci. U. S. A.*, vol. 110, no. 12, pp. 4780–4785, Mar. 2013, doi: 10.1073/pnas.1214546110.

[75] C. D. Marsden and J. D. Parkes, “‘ON-OFF’ EFFECTS IN PATIENTS WITH PARKINSON’S DISEASE ON CHRONIC LEVODOPA THERAPY,” *The Lancet*, vol. 307, no. 7954, pp. 292–296, Feb. 1976, doi: 10.1016/S0140-6736(76)91416-1.

[76] A. J. Lees, “The on-off phenomenon.,” *J. Neurol. Neurosurg. Psychiatry*, vol. 52, no. Suppl, pp. 29–37, Jun. 1989.

[77] G. C. Cotzias, P. S. Papavasiliou, and R. Gellene, “Modification of Parkinsonism--chronic treatment with L-dopa,” *N. Engl. J. Med.*, vol. 280, no. 7, pp. 337–345, Feb. 1969, doi: 10.1056/NEJM196902132800701.

[78] J. L. Vitek, “Deep brain stimulation: how does it work?,” *Cleve. Clin. J. Med.*, vol. 75 Suppl 2, pp. S59-65, Mar. 2008, doi: 10.3949/ccjm.75.suppl_2.s59.

[79] Y. Liu, N. Postupna, J. Falkenberg, and M. E. Anderson, “High frequency deep brain stimulation: What are the therapeutic mechanisms?,” *Neurosci. Biobehav. Rev.*, vol. 32, no. 3, pp. 343–351, Jan. 2008, doi: 10.1016/j.neubiorev.2006.10.007.

[80] A. Caramazza, A. Laudanna, and C. Romani, “Lexical access and inflectional morphology,” *Cognition*, vol. 28, no. 3, pp. 297–332, Apr. 1988, doi: 10.1016/0010-0277(88)90017-0.

[81] G. A. Ojemann, “Cortical organization of language,” *J. Neurosci. Off. J. Soc. Neurosci.*, vol. 11, no. 8, pp. 2281–2287, Aug. 1991.

[82] C. Wernicke, *Der aphasische Symptomenkomplex*. BreslauCohn & Weigert, 1874.

[83] N. Geschwind, “Disconnexion syndromes in animals and man. I,” *Brain J. Neurol.*, vol. 88, no. 2, pp. 237–294, Jun. 1965, doi: 10.1093/brain/88.2.237.

[84] M. P. Broca, “Remarques Sur le Siége de la Faculté Du Langage Articulé, Suivies D’une Observation D’aphémie,” *Bull. Soc. Anat.*, vol. 6, pp. 330–357, 1861.

[85] L. Lichtheim, “On aphasia,” *Brain*, no. 7, pp. 433–484, 1885.

[86] J. A. Fiez, D. A. Balota, M. E. Raichle, and S. E. Petersen, “Effects of lexicality, frequency, and spelling-to-sound consistency on the functional anatomy of reading,” *Neuron*, vol. 24, no. 1, pp. 205–218, Sep. 1999, doi: 10.1016/s0896-6273(00)80833-8.

[87] G. Hickok and D. Poeppel, “Dorsal and ventral streams: a framework for understanding aspects of the functional anatomy of language,” *Cognition*, vol. 92, no. 1–2, pp. 67–99, Jun. 2004, doi: 10.1016/j.cognition.2003.10.011.

[88] P. Indefrey and W. J. M. Levelt, “The spatial and temporal signatures of word production components,” *Cognition*, vol. 92, no. 1–2, pp. 101–144, Jun. 2004, doi: 10.1016/j.cognition.2002.06.001.

[89] M. W. Burton, S. L. Small, and S. E. Blumstein, “The role of segmentation in phonological processing: an fMRI investigation,” *J. Cogn. Neurosci.*, vol. 12, no. 4, pp. 679–690, Jul. 2000, doi: 10.1162/089892900562309.

[90] R. A. Poldrack, A. D. Wagner, M. W. Prull, J. E. Desmond, G. H. Glover, and J. D. Gabrieli, “Functional specialization for semantic and phonological processing in

the left inferior prefrontal cortex," *NeuroImage*, vol. 10, no. 1, pp. 15–35, Jul. 1999, doi: 10.1006/nimg.1999.0441.

[91] J. M. Anderson *et al.*, "Conduction aphasia and the arcuate fasciculus: A reexamination of the Wernicke-Geschwind model," *Brain Lang.*, vol. 70, no. 1, pp. 1–12, Oct. 1999, doi: 10.1006/brln.1999.2135.

[92] B. Bernal and A. Ardila, "The role of the arcuate fasciculus in conduction aphasia," *Brain J. Neurol.*, vol. 132, no. Pt 9, pp. 2309–2316, Sep. 2009, doi: 10.1093/brain/awp206.

[93] C. J. Price, "A review and synthesis of the first 20 years of PET and fMRI studies of heard speech, spoken language and reading," *NeuroImage*, vol. 62, no. 2, pp. 816–847, Aug. 2012, doi: 10.1016/j.neuroimage.2012.04.062.

[94] M. Papoutsi, J. A. de Zwart, J. M. Jansma, M. J. Pickering, J. A. Bednar, and B. Horwitz, "From Phonemes to Articulatory Codes: An fMRI Study of the Role of Broca's Area in Speech Production," *Cereb. Cortex N. Y. NY*, vol. 19, no. 9, pp. 2156–2165, Sep. 2009, doi: 10.1093/cercor/bhn239.

[95] F. H. Guenther, S. S. Ghosh, and J. A. Tourville, "Neural modeling and imaging of the cortical interactions underlying syllable production," *Brain Lang.*, vol. 96, no. 3, pp. 280–301, Mar. 2006, doi: 10.1016/j.bandl.2005.06.001.

[96] D. Callan, A. Callan, M. Gamez, M. Sato, and M. Kawato, "Premotor cortex mediates perceptual performance," *NeuroImage*, vol. 51, no. 2, pp. 844–858, Jun. 2010, doi: 10.1016/j.neuroimage.2010.02.027.

[97] B. R. Buchsbaum *et al.*, "Conduction aphasia, sensory-motor integration, and phonological short-term memory - an aggregate analysis of lesion and fMRI data," *Brain Lang.*, vol. 119, no. 3, pp. 119–128, Dec. 2011, doi: 10.1016/j.bandl.2010.12.001.

[98] H. Axer, A. G. von Keyserlingk, G. Berks, and D. G. von Keyserlingk, "Supra- and infrasylvian conduction aphasia," *Brain Lang.*, vol. 76, no. 3, pp. 317–331, Mar. 2001, doi: 10.1006/brln.2000.2425.

[99] H. Damasio and A. R. Damasio, "The anatomical basis of conduction aphasia," *Brain J. Neurol.*, vol. 103, no. 2, pp. 337–350, Jun. 1980, doi: 10.1093/brain/103.2.337.

[100] J. Fridriksson *et al.*, "Impaired speech repetition and left parietal lobe damage," *J. Neurosci. Off. J. Soc. Neurosci.*, vol. 30, no. 33, pp. 11057–11061, Aug. 2010, doi: 10.1523/JNEUROSCI.1120-10.2010.

[101] S. B. Pillay, B. C. Stengel, C. Humphries, D. S. Book, and J. R. Binder, “Cerebral localization of impaired phonological retrieval during rhyme judgment,” *Ann. Neurol.*, vol. 76, no. 5, pp. 738–746, Nov. 2014, doi: 10.1002/ana.24266.

[102] J. R. Binder, “The Wernicke area,” *Neurology*, vol. 85, no. 24, pp. 2170–2175, Dec. 2015, doi: 10.1212/WNL.0000000000002219.

[103] L. Bartha and T. Benke, “Acute conduction aphasia: an analysis of 20 cases,” *Brain Lang.*, vol. 85, no. 1, pp. 93–108, Apr. 2003, doi: 10.1016/s0093-934x(02)00502-3.

[104] R. Brookshire, *Introduction to neurogenic communication disorders*, 6th ed. St. Louis: Mosby Year Book, 2003.

[105] F.-E. Roux, J.-B. Durand, M. Jucla, E. Réhault, M. Reddy, and J.-F. Démonet, “Segregation of lexical and sub-lexical reading processes in the left perisylvian cortex,” *PloS One*, vol. 7, no. 11, p. e50665, 2012, doi: 10.1371/journal.pone.0050665.

[106] M. L. Gorno-Tempini *et al.*, “The logopenic/phonological variant of primary progressive aphasia,” *Neurology*, vol. 71, no. 16, pp. 1227–1234, Oct. 2008, doi: 10.1212/01.wnl.0000320506.79811.da.

[107] M. L. Gorno-Tempini *et al.*, “Classification of primary progressive aphasia and its variants,” *Neurology*, vol. 76, no. 11, pp. 1006–1014, Mar. 2011, doi: 10.1212/WNL.0b013e31821103e6.

[108] I. DeWitt and J. P. Rauschecker, “Phoneme and word recognition in the auditory ventral stream,” *Proc. Natl. Acad. Sci. U. S. A.*, vol. 109, no. 8, pp. E505-514, Feb. 2012, doi: 10.1073/pnas.1113427109.

[109] J. R. Binder *et al.*, “Human temporal lobe activation by speech and nonspeech sounds,” *Cereb. Cortex N. Y. N 1991*, vol. 10, no. 5, pp. 512–528, May 2000, doi: 10.1093/cercor/10.5.512.

[110] S. A. Shimamoto, E. S. Ryapolova-Webb, J. L. Ostrem, N. B. Galifianakis, K. J. Miller, and P. A. Starr, “Subthalamic nucleus neurons are synchronized to primary motor cortex local field potentials in Parkinson’s disease,” *J. Neurosci. Off. J. Soc. Neurosci.*, vol. 33, no. 17, pp. 7220–7233, Apr. 2013, doi: 10.1523/JNEUROSCI.4676-12.2013.

[111] J. Z. Jin *et al.*, “ON AND OFF DOMAINS OF GENICULATE AFFERENTS IN CAT PRIMARY VISUAL CORTEX,” *Nat. Neurosci.*, vol. 11, no. 1, pp. 88–94, Jan. 2008, doi: 10.1038/nn2029.

[112] I. Nauhaus, L. Busse, M. Carandini, and D. L. Ringach, “Stimulus contrast modulates functional connectivity in visual cortex,” *Nat. Neurosci.*, vol. 12, no. 1, pp. 70–76, Jan. 2009, doi: 10.1038/nn.2232.

[113] S. Ray and J. H. R. Maunsell, “Network rhythms influence the relationship between spike-triggered local field potential and functional connectivity,” *J. Neurosci. Off. J. Soc. Neurosci.*, vol. 31, no. 35, pp. 12674–12682, Aug. 2011, doi: 10.1523/JNEUROSCI.1856-11.2011.

[114] D. Khodagholy *et al.*, “NeuroGrid: recording action potentials from the surface of the brain,” *Nat. Neurosci.*, vol. 18, no. 2, pp. 310–315, Feb. 2015, doi: 10.1038/nn.3905.

[115] S. Shoham, M. R. Fellows, and R. A. Normann, “Robust, automatic spike sorting using mixtures of multivariate t-distributions,” *J. Neurosci. Methods*, vol. 127, no. 2, pp. 111–122, Aug. 2003, doi: 10.1016/s0165-0270(03)00120-1.

[116] B. L. Sabatini and W. G. Regehr, “Timing of neurotransmission at fast synapses in the mammalian brain,” *Nature*, vol. 384, no. 6605, pp. 170–172, Nov. 1996, doi: 10.1038/384170a0.

[117] G. M. Shepherd, *The Synaptic Organization of the Brain*. Oxford University Press, 2004. Accessed: Dec. 08, 2019. [Online]. Available: https://www.oxfordscholarship.com/view/10.1093/acprof:oso/9780195159561.001.1/acprof-9780195159561

[118] K. Koch, J. McLean, M. Berry, P. Sterling, V. Balasubramanian, and M. A. Freed, “Efficiency of information transmission by retinal ganglion cells,” *Curr. Biol. CB*, vol. 14, no. 17, pp. 1523–1530, Sep. 2004, doi: 10.1016/j.cub.2004.08.060.

[119] S. Moshel *et al.*, “Subthalamic nucleus long-range synchronization-an independent hallmark of human Parkinson’s disease,” *Front. Syst. Neurosci.*, vol. 7, p. 79, 2013, doi: 10.3389/fnsys.2013.00079.

[120] J.-S. Brittain and P. Brown, “Oscillations and the basal ganglia: Motor control and beyond,” *NeuroImage*, vol. 85, pp. 637–647, Jan. 2014, doi: 10.1016/j.neuroimage.2013.05.084.

[121] M. J. Rojas, J. A. Navas, and D. M. Rector, “Evoked response potential markers for anesthetic and behavioral states,” *Am. J. Physiol. Regul. Integr. Comp. Physiol.*, vol. 291, no. 1, pp. R189-196, Jul. 2006, doi: 10.1152/ajpregu.00409.2005.

[122] S. Potez and M. E. Larkum, “Effect of common anesthetics on dendritic properties in layer 5 neocortical pyramidal neurons,” *J. Neurophysiol.*, vol. 99, no. 3, pp. 1394–1407, Mar. 2008, doi: 10.1152/jn.01126.2007.

[123] X. Liu, K. K. Lauer, B. D. Ward, S.-J. Li, and A. G. Hudetz, "Differential effects of deep sedation with propofol on the specific and nonspecific thalamocortical systems: a functional magnetic resonance imaging study," *Anesthesiology*, vol. 118, no. 1, pp. 59–69, Jan. 2013, doi: 10.1097/ALN.0b013e318277a801.

[124] M. M. McCarthy, E. N. Brown, and N. Kopell, "Potential network mechanisms mediating electroencephalographic beta rhythm changes during propofol-induced paradoxical excitation," *J. Neurosci. Off. J. Soc. Neurosci.*, vol. 28, no. 50, pp. 13488–13504, Dec. 2008, doi: 10.1523/JNEUROSCI.3536-08.2008.

[125] A. Bollimunta, Y. Chen, C. E. Schroeder, and M. Ding, "Neuronal Mechanisms of Cortical Alpha Oscillations in Awake-Behaving Macaques," *J. Neurosci.*, vol. 28, no. 40, pp. 9976–9988, Oct. 2008, doi: 10.1523/JNEUROSCI.2699-08.2008.

[126] F. Clascá, P. Rubio-Garrido, and D. Jabaudon, "Unveiling the diversity of thalamocortical neuron subtypes," *Eur. J. Neurosci.*, vol. 35, no. 10, pp. 1524–1532, May 2012, doi: 10.1111/j.1460-9568.2012.08033.x.

[127] L. I. Schmitt, R. D. Wimmer, M. Nakajima, M. Happ, S. Mofakham, and M. M. Halassa, "Thalamic amplification of cortical connectivity sustains attentional control," *Nature*, vol. 545, no. 7653, pp. 219–223, 11 2017, doi: 10.1038/nature22073.

[128] E. Kuramoto *et al.*, "Individual mediodorsal thalamic neurons project to multiple areas of the rat prefrontal cortex: A single neuron-tracing study using virus vectors," *J. Comp. Neurol.*, vol. 525, no. 1, pp. 166–185, 01 2017, doi: 10.1002/cne.24054.

[129] C. de Hemptinne *et al.*, "Therapeutic deep brain stimulation reduces cortical phase-amplitude coupling in Parkinson's disease," *Nat. Neurosci.*, vol. 18, no. 5, pp. 779–786, May 2015, doi: 10.1038/nn.3997.

[130] M. Nakajima and M. M. Halassa, "Thalamic control of functional cortical connectivity," *Curr. Opin. Neurobiol.*, vol. 44, pp. 127–131, 2017, doi: 10.1016/j.conb.2017.04.001.

[131] V. S. Sohal, "How Close Are We to Understanding What (if Anything) γ Oscillations Do in Cortical Circuits?," *J. Neurosci. Off. J. Soc. Neurosci.*, vol. 36, no. 41, pp. 10489–10495, 12 2016, doi: 10.1523/JNEUROSCI.0990-16.2016.

[132] A. Gunduz *et al.*, "Proceedings of the Second Annual Deep Brain Stimulation Think Tank: What's in the Pipeline," *Int. J. Neurosci.*, vol. 125, no. 7, pp. 475–485, 2015, doi: 10.3109/00207454.2014.999268.

[133] D. Williams *et al.*, "Dopamine-dependent changes in the functional connectivity between basal ganglia and cerebral cortex in humans," *Brain J. Neurol.*, vol. 125, no. Pt 7, pp. 1558–1569, Jul. 2002, doi: 10.1093/brain/awf156.

[134] B. Picconi *et al.*, “Loss of bidirectional striatal synaptic plasticity in L-DOPA-induced dyskinesia,” *Nat. Neurosci.*, vol. 6, no. 5, pp. 501–506, May 2003, doi: 10.1038/nn1040.

[135] D. B. Shalom and D. Poeppel, “Functional anatomic models of language: assembling the pieces,” *Neurosci. Rev. J. Bringing Neurobiol. Neurol. Psychiatry*, vol. 14, no. 1, pp. 119–127, Feb. 2008, doi: 10.1177/1073858407305726.

[136] J. S. Brumberg, A. Nieto-Castanon, P. R. Kennedy, and F. H. Guenther, “Brain-Computer Interfaces for Speech Communication,” *Speech Commun.*, vol. 52, no. 4, pp. 367–379, Apr. 2010, doi: 10.1016/j.specom.2010.01.001.

[137] J. S. Brumberg, E. J. Wright, D. S. Andreasen, F. H. Guenther, and P. R. Kennedy, “Classification of intended phoneme production from chronic intracortical microelectrode recordings in speech-motor cortex,” *Front. Neurosci.*, vol. 5, p. 65, 2011, doi: 10.3389/fnins.2011.00065.

[138] A. M. Chan *et al.*, “Speech-specific tuning of neurons in human superior temporal gyrus,” *Cereb. Cortex N. Y. N 1991*, vol. 24, no. 10, pp. 2679–2693, Oct. 2014, doi: 10.1093/cercor/bht127.

[139] Q. Rabbani, G. Milsap, and N. E. Crone, “The Potential for a Speech Brain-Computer Interface Using Chronic Electrocorticography,” *Neurother. J. Am. Soc. Exp. Neurother.*, vol. 16, no. 1, pp. 144–165, 2019, doi: 10.1007/s13311-018-00692-2.

[140] C. J. Stam, G. Nolte, and A. Daffertshofer, “Phase lag index: assessment of functional connectivity from multi channel EEG and MEG with diminished bias from common sources,” *Hum. Brain Mapp.*, vol. 28, no. 11, pp. 1178–1193, Nov. 2007, doi: 10.1002/hbm.20346.

[141] M. Vinck, R. Oostenveld, M. van Wingerden, F. Battaglia, and C. M. A. Pennartz, “An improved index of phase-synchronization for electrophysiological data in the presence of volume-conduction, noise and sample-size bias,” *NeuroImage*, vol. 55, no. 4, pp. 1548–1565, Apr. 2011, doi: 10.1016/j.neuroimage.2011.01.055.

[142] J. M. Hurtado, L. L. Rubchinsky, and K. A. Sigvardt, “Statistical method for detection of phase-locking episodes in neural oscillations,” *J. Neurophysiol.*, vol. 91, no. 4, pp. 1883–1898, Apr. 2004, doi: 10.1152/jn.00853.2003.

[143] B. R. Buchsbaum, G. Hickok, and C. Humphries, “Role of left posterior superior temporal gyrus in phonological processing for speech perception and production,” *Cogn. Sci.*, vol. 25, no. 5, pp. 663–678, 2001, doi: 10.1207/s15516709cog2505_2.

[144] G. Hickok, “The functional neuroanatomy of language,” *Phys. Life Rev.*, vol. 6, no. 3, pp. 121–143, Sep. 2009, doi: 10.1016/j.plrev.2009.06.001.

[145] N. T. Sahin, S. Pinker, S. S. Cash, D. Schomer, and E. Halgren, “Sequential processing of lexical, grammatical, and phonological information within Broca’s area,” *Science*, vol. 326, no. 5951, pp. 445–449, Oct. 2009, doi: 10.1126/science.1174481.

[146] P. Indefrey, “The Spatial and Temporal Signatures of Word Production Components: A Critical Update,” *Front. Psychol.*, vol. 2, Oct. 2011, doi: 10.3389/fpsyg.2011.00255.

[147] K. E. Bouchard, N. Mesgarani, K. Johnson, and E. F. Chang, “Functional Organization of Human Sensorimotor Cortex for Speech Articulation,” *Nature*, vol. 495, no. 7441, pp. 327–332, Mar. 2013, doi: 10.1038/nature11911.

[148] R. Salmelin, R. Hari, O. V. Lounasmaa, and M. Sams, “Dynamics of brain activation during picture naming,” *Nature*, vol. 368, no. 6470, Art. no. 6470, Mar. 1994, doi: 10.1038/368463a0.

[149] W. J. M. Levelt, P. Praamstra, A. S. Meyer, P. Helenius, and R. Salmelin, “An MEG Study of Picture Naming,” *J. Cogn. Neurosci.*, vol. 10, no. 5, pp. 553–567, Sep. 1998, doi: 10.1162/089892998562960.

[150] P. Sörös, K. Cornelissen, M. Laine, and R. Salmelin, “Naming actions and objects: cortical dynamics in healthy adults and in an anomic patient with a dissociation in action/object naming,” *NeuroImage*, vol. 19, no. 4, pp. 1787–1801, Aug. 2003, doi: 10.1016/S1053-8119(03)00217-9.

[151] A. Hultén, M. Vihla, M. Laine, and R. Salmelin, “Accessing newly learned names and meanings in the native language,” *Hum. Brain Mapp.*, vol. 30, no. 3, pp. 976–989, Mar. 2009, doi: 10.1002/hbm.20561.

[152] M. Vihla, M. Laine, and R. Salmelin, “Cortical dynamics of visual/semantic vs. phonological analysis in picture confrontation,” *NeuroImage*, vol. 33, no. 2, pp. 732–738, Nov. 2006, doi: 10.1016/j.neuroimage.2006.06.040.

[153] T. Schuhmann, N. O. Schiller, R. Goebel, and A. T. Sack, “The temporal characteristics of functional activation in Broca’s area during overt picture naming,” *Cortex J. Devoted Study Nerv. Syst. Behav.*, vol. 45, no. 9, pp. 1111–1116, Oct. 2009, doi: 10.1016/j.cortex.2008.10.013.

[154] B. N. Pasley and R. T. Knight, “Decoding speech for understanding and treating aphasia,” *Prog. Brain Res.*, vol. 207, pp. 435–456, 2013, doi: 10.1016/B978-0-444-63327-9.00018-7.

[155] A. Stuart, J. Kalinowski, M. P. Rastatter, and K. Lynch, “Effect of delayed auditory feedback on normal speakers at two speech rates,” *J. Acoust. Soc. Am.*, vol. 111, no. 5 Pt 1, pp. 2237–2241, May 2002, doi: 10.1121/1.1466868.

[156] H. Chon, S. J. Kraft, J. Zhang, T. Loucks, and N. G. Ambrose, “Individual variability in delayed auditory feedback effects on speech fluency and rate in normally fluent adults,” *J. Speech Lang. Hear. Res. JSLHR*, vol. 56, no. 2, pp. 489–504, Apr. 2013, doi: 10.1044/1092-4388(2012/11-0303).

[157] C. J. D. Hardy *et al.*, “Sensitivity of Speech Output to Delayed Auditory Feedback in Primary Progressive Aphasias,” *Front. Neurol.*, vol. 9, Oct. 2018, doi: 10.3389/fneur.2018.00894.

[158] G. Andrews, P. M. Howie, M. Dozsa, and B. E. Guitar, “Stuttering: speech pattern characteristics under fluency-inducing conditions,” *J. Speech Hear. Res.*, vol. 25, no. 2, pp. 208–216, Jun. 1982.

[159] A. L. Foundas, J. R. Mock, D. M. Corey, E. J. Golob, and E. G. Conture, “The SpeechEasy device in stuttering and nonstuttering adults: fluency effects while speaking and reading,” *Brain Lang.*, vol. 126, no. 2, pp. 141–150, Aug. 2013, doi: 10.1016/j.bandl.2013.04.004.

[160] I.-F. Lin, T. Mochida, K. Asada, S. Ayaya, S.-I. Kumagaya, and M. Kato, “Atypical delayed auditory feedback effect and Lombard effect on speech production in high-functioning adults with autism spectrum disorder,” *Front. Hum. Neurosci.*, vol. 9, Sep. 2015, doi: 10.3389/fnhum.2015.00510.

[161] B. S. Lee, “Effects of Delayed Speech Feedback,” *J. Acoust. Soc. Am.*, vol. 22, no. 6, pp. 824–826, Nov. 1950, doi: 10.1121/1.1906696.

[162] P. Howell, “Effects of delayed auditory feedback and frequency-shifted feedback on speech control and some potentials for future development of prosthetic aids for stammering,” *Stammering Res. -Line J. Publ. Br. Stammering Assoc.*, vol. 1, no. 1, pp. 31–46, Apr. 2004.

[163] M. E. Linn-Evans *et al.*, “REM sleep without atonia is associated with increased rigidity in patients with mild to moderate Parkinson’s disease,” *Clin. Neurophysiol.*, vol. 131, no. 8, pp. 2008–2016, Aug. 2020, doi: 10.1016/j.clinph.2020.04.017.

[164] A. Westbrook and T. S. Braver, “Cognitive effort: A neuroeconomic approach,” *Cogn. Affect. Behav. Neurosci.*, vol. 15, no. 2, pp. 395–415, Jun. 2015, doi: 10.3758/s13415-015-0334-y.

[165] J. E. Aman *et al.*, “Directional deep brain stimulation leads reveal spatially distinct oscillatory activity in the globus pallidus internus of Parkinson’s disease patients,” *Neurobiol. Dis.*, vol. 139, p. 104819, Jun. 2020, doi: 10.1016/j.nbd.2020.104819.